ACS APPLIED MATERIALS & INTERFACES

Research Article

Cite This: ACS Appl. Mater. Interfaces XXXX, XXX, XXX-XXX

www.acsami.org

Design of Lubricant Infused Surfaces

Daniel J. Preston, Youngsup Song, Zhengmao Lu, Dion S. Antao, and Evelyn N. Wang*

Department of Mechanical Engineering, Massachusetts Institute of Technology, 77 Massachusetts Avenue, Cambridge, Massachusetts 02139, United States

Supporting Information

ABSTRACT: Lubricant infused surfaces (LIS) are a recently developed and promising approach to fluid repellency for applications in biology, microfluidics, thermal management, lab-on-a-chip, and beyond. The design of LIS has been explored in past work in terms of surface energies, which need to be determined empirically for each interface in a given system. Here, we developed an approach that predicts a priori whether an arbitrary combination of solid and lubricant will repel a given impinging fluid. This model was validated with experiments performed in our work as well as in literature and was subsequently used to develop a new framework for LIS with distinct design guidelines. Furthermore, insights gained from the model led to the experimental demonstration of LIS using uncoated high-surface-energy solids, thereby eliminating the need for unreliable low-surface-energy coatings and resulting in LIS repelling the lowest surface tension impinging fluid (butane, $\gamma \approx 13$ mN/m) reported to date.

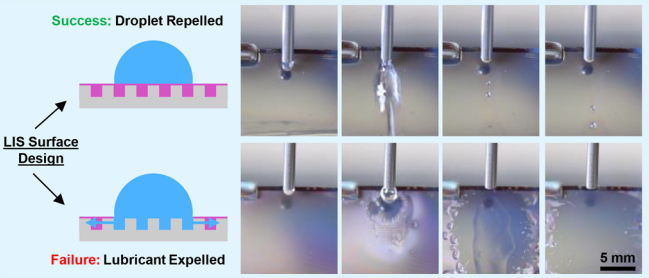

KEYWORDS: *surface engineering, slippery materials, bioinspired surfaces, interfacial phenomena, soft materials, surface energy, fluid repellency*

INTRODUCTION

Lubricant infused surfaces (LIS) have risen to prominence in micro- and nanoscale research,[1] fluid dynamics,[2] heat transfer,[3,4] biology,[5] and lab-on-a-chip[6] due to their impressive ability to shed impinging droplets. LIS comprise a textured solid surface into which a lubricant is "infused", or spontaneously wicked, and on which an impinging fluid ideally forms discrete droplets which easily shed from the surface. Conceived in 1959[7] and explored briefly in subsequent work,[8,9] the significance of LIS has only more recently been recognized through developments reported independently by LaFuma and Quéré[10] and Wong et al.[11] in 2011. Since then, applications have spanned from condensation enhancement,[12−14] to anti-icing,[15] and even paper-based microfluidics.[16] LIS have also been shown to exhibit the ability to repel low surface tension fluids (as low as 17 mN/m),[11,17] which is critical for applications in thermal management and hydrocarbon processing.

The design of these surfaces, specifically the choice of a rough solid and a lubricant for a given impinging fluid based on energetic considerations, is well-understood.[10,11,18] LIS need to meet the following criteria: the impinging fluid must be immiscible with the lubricant; the lubricant must wet the solid structures both with and without the impinging fluid present; and the impinging fluid must form discrete droplets on the LIS as opposed to a continuous film. On the basis of this understanding, all of the works on LIS design have presented models that require either contact angles or spreading coefficients of the impinging fluid and lubricant on the solid surface, as well as the interfacial tension between the lubricant and the impinging fluid. Unfortunately, these properties have been measured empirically and used to justify LIS behavior after experiments with LIS were already conducted. Predictive capability has not been possible for combinations of fluids and solids where empirical knowledge of all of the interfacial energies in the system is not readily available.

Here, we present an approach to determine a priori whether an arbitrary combination of solid and lubricant will repel a given impinging fluid. This model predicts the unknown surface energies in the system on the basis of the method proposed by van Oss, Chaudhury, and Good (vOCG).[19] We validate this model against experiments performed in the present work as well as in the literature, through which we show excellent predictive capability. With this framework for LIS design, we show that LIS on uncoated high-surface-energy solids are possible, thereby eliminating the need for unreliable[20] low-surface-energy coatings typically used. Furthermore, we experimentally demonstrate repulsion of the lowest surface tension impinging fluid (butane, $\gamma \approx 13$ mN/m) reported using a LIS, which in this case comprised an uncoated high-surface-energy solid (silicon dioxide) with a fluorinated but highly polar lubricant (hexafluoroisopropanol).

Received: September 20, 2017
Accepted: November 9, 2017
Published: November 9, 2017

DOI: 10.1021/acsami.7b14311
ACS Appl. Mater. Interfaces XXXX, XXX, XXX−XXX

PREDICTIVE LIS MODEL

LIS behavior is governed by the interfacial interactions between the three condensed phases (solid, lubricant, and impinging fluid, with each other and with the surrounding environment) and by the geometry of the solid surface. These interfacial interactions and the surface geometry can be used to predict whether a LIS will successfully repel an impinging fluid as discrete droplets. The geometry of the solid surface is described by the roughness, r, which represents the actual solid surface area divided by the projected area, and the solid fraction, φ, which represents the fraction of the solid that contacts the base of an impinging droplet; these properties are combined here as the geometric factor $R = (r - 1)/(r - \varphi)$, where R can vary from 0 for a flat surface to 1 for an extremely rough surface. Meanwhile, the interfacial interactions can be described at a high level by the surface energies of the three phases with the surrounding vapor and either the contact angles or the spreading parameters of the three phases with each other.

The criteria that must be met for a functional LIS can be considered in terms of the spreading parameters S_{xy} for each interface in the system, where the first and second subscripts of S_{xy} refer to the spreading phase and the reference phase, respectively. If the total energy required for the reference phase to be covered by a layer of the spreading phase is negative, indicating spontaneous coverage of the reference phase by the spreading phase, the spreading parameter is positive. Accordingly, the spreading parameter is defined as $S_{xy} = \gamma_y - (\gamma_{xy} + \gamma_x)$, where γ_x and γ_y are the surface energies of phases x and y with the surroundings and γ_{xy} is the interfacial energy between phases x and y. In the following discussion regarding LIS, the subscript l refers to the lubricant, d is the impinging fluid droplet, and s is the solid. When a single symbol appears in the subscript, it refers to the interface of that phase with its own vapor. Two symbols appearing in the same subscript indicate an interface between two phases, with the symbols referring to the two phases; in the case of the spreading coefficient, the first symbol is the spreading phase and the second symbol is the reference phase.

In the ideal case, the impinging fluid forms a discrete droplet on the LIS and the lubricant remains trapped within the rough solid structured surface beneath the droplet. If criterion (I):

$$S_{ld} < 0 \tag{1}$$

is not met and the spreading parameter for the lubricant on the droplet is positive, the lubricant spontaneously spreads over and "cloaks" the droplet as shown in Figure 1. The cloaked droplet retains most of the functionality of a noncloaked droplet on the LIS (high mobility, etc.), but the cloaked state is still generally undesirable due to the removal of lubricant when droplets depart from the surface, depleting the lubricant over time. If criterion (II):

$$S_{dl} < 0 \tag{2}$$

is not met, the impinging fluid spreads indefinitely over the lubricant, resulting in formation of a film instead of discrete droplets and subsequent failure of the LIS. If criteria (III) and (IV):

$$S_{ls} > -\gamma_l R \tag{3}$$

$$S_{ls(d)} > -\gamma_{dl} R \tag{4}$$

are not met, the lubricant does not spread within the rough structured solid surface during operation (the subscript (d) in criterion (IV) means "in the presence of the impinging droplet"). Specifically, when criterion (III) is not met, the lubricant does not infuse in the solid structures in the presence of the surrounding vapor, and when criterion (IV) is not met, the lubricant does not infuse in the solid structures in the presence of the impinging fluid, either of which results in failure of the LIS. If the spreading coefficients S_{ls} and $S_{ls(d)}$ in the inequalities in criteria (III) and (IV) exceed zero, the lubricant fully covers the solid surface in the presence of the vapor or the impinging fluid, respectively, as opposed to leaving the tops of the rough solid structures exposed. The case where the structures are completely covered by lubricant results in significantly reduced contact angle hysteresis, as described in detail in past work, but is not necessary for a stable LIS.[18] Finally, if criterion (V):

$$\gamma_{dl} > 0 \tag{5}$$

is not met, the interface between the lubricant and the impinging fluid increases its surface area indefinitely to minimize energy, ultimately resulting in the miscibility of the two fluids; criterion (V) has not been expressed quantitatively in previous literature on LIS.

The interfacial energies between any two condensed phases in these criteria, γ_{dl}, γ_{ls}, and γ_{ds}, are not typically tabulated for the majority of interfacial interactions of interest and therefore have only been obtained experimentally for the phases considered in prior work on LIS. Here, we unify the above energy-based criteria with a model that can predict the unknown interfacial energies to gain new insight into LIS surface design and additionally reduce the time required to experimentally characterize a given combination of N materials from $O(N^3)$ to $O(N)$; for example, this method results in a reduction in the number of required experiments by 2 orders of

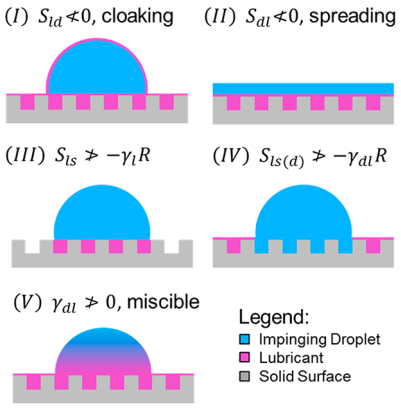

Figure 1. Failure modes predicted from surface-energy-based criteria for LIS design. The ideal droplet of impinging fluid on a LIS rests atop a combined lubricant-solid layer. If criterion (I) is not satisfied, the droplet will be "cloaked", or covered with a thin layer of lubricant, which may eventually deplete the surface of lubricant as droplets depart. The impinging fluid will spread over the LIS as a film if criterion (II) is not met. Criteria (III) and (IV) must be met to ensure that the lubricant remains infused in the rough solid. If S_{ls} or $S_{ls(d)}$ is greater than zero, the lubricant will cover the entire surface in the presence of the vapor or condensate, respectively; otherwise, if (III) or (IV) are still satisfied but S_{ls} or $S_{ls(d)}$ is less than zero, a fraction φ of the solid will contact the impinging fluid in the presence of the vapor or condensate, respectively. Miscibility of the impinging fluid and the lubricant is characterized by the interfacial tension between these two fluids, where if criterion (V) is not met, it is energetically favorable for the two fluids to form an infinitely large interface (i.e., fully mix).

DOI: 10.1021/acsami.7b14311
ACS Appl. Mater. Interfaces XXXX, XXX, XXX−XXX

magnitude when considering combinations of 30 impinging fluids, lubricants, and solids (see the Supporting Information). We start with Fowkes' assumption that an interfacial energy can be divided into contributions from various intermolecular forces, for example, dispersive, polar, metallic, etc., and then predict these components independently from properties of the interacting phases.[21,22] The dispersive (or London) forces are combined with induced dipole and permanent dipole forces and termed the Lifshitz–van der Waals (LW) component of interfacial energy, which can be determined on the basis of physical first-principles with reasonable confidence from a geometric combining rule.[21,22] The polar component was initially treated in the same manner by Owens and Wendt (OW),[23] but this method is now considered obsolete and has been largely replaced by the more accurate method proposed by van Oss, Chaudhury, and Good (vOCG)[19,24−26] in which Lewis acid–base contributions to interfacial energy are considered. The vOCG method outperforms the OW method most notably in cases were hydrogen bonding is involved, and is also considered more versatile than the commonly used Neumann method;[27] as such, the vOCG method is used here to predict the polar contribution to interfacial energy between condensed phases.[26−28] Metallic interactions are not considered here, but would need to be considered to account for interactions between phases such as mercury and metallic solids.

For any given phase "A", the total interfacial energy is found from the LW and acid–base components as shown in eq 6, where the geometric mean of the vOCG acid–base terms yields the polar interaction (acid term represented by superscript "+", base represented by superscript "−"). The interfacial tension between two phases (A and B) is found from eq 7, where each fluid's LW and acid–base terms are considered. Note that when phases A and B have identical LW and acid–base terms (i.e., they are the same fluid), the interfacial energy recovered from eq 7 is zero as expected.

$$\gamma_A^{total} = \gamma_A^{LW} + 2\sqrt{\gamma_A^+\gamma_A^-} \tag{6}$$

$$\gamma_{AB}^{total} = \gamma_A^{LW} + \gamma_B^{LW} - 2\sqrt{\gamma_A^{LW}\gamma_B^{LW}} + 2\sqrt{\gamma_A^+\gamma_A^-} + 2\sqrt{\gamma_B^+\gamma_B^-} - 2\sqrt{\gamma_A^+\gamma_B^-} - 2\sqrt{\gamma_B^+\gamma_A^-} \tag{7}$$

Equation 7 is used to predict the three interfacial energies between condensed phases, γ_{dl}, γ_{ls}, and γ_{ds}, used in criteria (I)–(V) shown in Figure 1. The expanded forms of criteria (I)–(V), substituting eqs 6 and 7 into eqs 1–5, are presented in eqs 8–12, respectively:

Criterion (I):

$$\begin{aligned} S_{ld} &= \gamma_d - (\gamma_{dl} + \gamma_l) \\ &= \gamma_d^{LW} + 2\sqrt{\gamma_d^+\gamma_d^-} - \gamma_l^{LW} - 2\sqrt{\gamma_l^+\gamma_l^-} - \gamma_d^{LW} - \gamma_l^{LW} \\ &\quad + 2\sqrt{\gamma_d^{LW}\gamma_l^{LW}} - 2\sqrt{\gamma_d^+\gamma_d^-} - 2\sqrt{\gamma_l^+\gamma_l^-} + 2\sqrt{\gamma_d^+\gamma_l^-} \\ &\quad + 2\sqrt{\gamma_l^+\gamma_d^-} < 0 \end{aligned} \tag{8}$$

Criterion (II):

$$\begin{aligned} S_{dl} &= \gamma_l - (\gamma_{dl} + \gamma_d) \\ &= \gamma_l^{LW} + 2\sqrt{\gamma_l^+\gamma_l^-} - \gamma_d^{LW} - 2\sqrt{\gamma_d^+\gamma_d^-} - \gamma_d^{LW} - \gamma_l^{LW} \\ &\quad + 2\sqrt{\gamma_d^{LW}\gamma_l^{LW}} - 2\sqrt{\gamma_d^+\gamma_d^-} - 2\sqrt{\gamma_l^+\gamma_l^-} + 2\sqrt{\gamma_d^+\gamma_l^-} \\ &\quad + 2\sqrt{\gamma_l^+\gamma_d^-} < 0 \end{aligned} \tag{9}$$

Criterion (III):

$$\begin{aligned} S_{ls} + \gamma_l R &= \gamma_s - (\gamma_{ls} + \gamma_l) + \gamma_l R \\ &= \gamma_s^{LW} + 2\sqrt{\gamma_s^+\gamma_s^-} - \gamma_l^{LW} - \gamma_s^{LW} + 2\sqrt{\gamma_l^{LW}\gamma_s^{LW}} \\ &\quad - 2\sqrt{\gamma_l^+\gamma_l^-} - 2\sqrt{\gamma_s^+\gamma_s^-} + 2\sqrt{\gamma_l^+\gamma_s^-} + 2\sqrt{\gamma_s^+\gamma_l^-} + \\ &\quad (R-1)(\gamma_l^{LW} + 2\sqrt{\gamma_l^+\gamma_l^-}) > 0 \end{aligned} \tag{10}$$

Criterion (IV):

$$\begin{aligned} S_{ls(d)} + \gamma_{dl} R &= \gamma_{ds} - (\gamma_{ls} + \gamma_{dl}) + \gamma_{dl} R \\ &= \gamma_d^{LW} + \gamma_s^{LW} - 2\sqrt{\gamma_d^{LW}\gamma_s^{LW}} + 2\sqrt{\gamma_d^+\gamma_d^-} + 2\sqrt{\gamma_s^+\gamma_s^-} \\ &\quad - 2\sqrt{\gamma_d^+\gamma_s^-} - 2\sqrt{\gamma_s^+\gamma_d^-} - \gamma_l^{LW} - \gamma_s^{LW} + 2\sqrt{\gamma_l^{LW}\gamma_s^{LW}} \\ &\quad - 2\sqrt{\gamma_l^+\gamma_l^-} - 2\sqrt{\gamma_s^+\gamma_s^-} + 2\sqrt{\gamma_l^+\gamma_s^-} + 2\sqrt{\gamma_s^+\gamma_l^-} \\ &\quad + (R-1)(\gamma_d^{LW} + \gamma_l^{LW} - 2\sqrt{\gamma_d^{LW}\gamma_l^{LW}} + 2\sqrt{\gamma_d^+\gamma_d^-} \\ &\quad + 2\sqrt{\gamma_l^+\gamma_l^-} - 2\sqrt{\gamma_d^+\gamma_l^-} - 2\sqrt{\gamma_l^+\gamma_d^-}) > 0 \end{aligned} \tag{11}$$

Criterion (V):

$$\begin{aligned} \gamma_{dl} &= \gamma_d^{LW} + \gamma_l^{LW} - 2\sqrt{\gamma_d^{LW}\gamma_l^{LW}} + 2\sqrt{\gamma_d^+\gamma_d^-} + 2\sqrt{\gamma_l^+\gamma_l^-} \\ &\quad - 2\sqrt{\gamma_d^+\gamma_l^-} - 2\sqrt{\gamma_l^+\gamma_d^-} > 0 \end{aligned} \tag{12}$$

These inequalities provide information enabling the design and functionality of LIS. An interesting example is the design of LIS to repel low surface tension fluids such as refrigerants or hydrocarbons, which are often nonpolar. In the case of a nonpolar impinging fluid ($\gamma_d^+ = \gamma_d^- = 0$), to avoid both cloaking (criterion I, eq 8) and spreading of the impinging fluid on the LIS (criterion II, eq 9), the combined inequality in eq 13 must be satisfied. Therefore, it is impossible to meet both criteria I and II if the lubricant is also nonpolar; the lubricant must have some polar component of surface energy to avoid both cloaking and spreading of the impinging fluid.

$$\sqrt{\gamma_l^{LW}} + \frac{\sqrt{\gamma_l^+\gamma_l^-}}{\sqrt{\gamma_l^{LW}}} > \sqrt{\gamma_d^{LW}} > \sqrt{\gamma_l^{LW}} \tag{13}$$

There are limitations to the vOCG method when used for the prediction of interfacial energies. Several specific concerns raised are that the base components are systematically greater than the acid components,[29] that experimentally determined surface energy components may depend on the set of fluids chosen for experiments,[29] and that the values of the components may sometimes take negative values.[24,29] In response to the first concern, the relative magnitudes of the acid and base terms are set by the choice of the components of water, which are typically equal to each other but may be chosen to make typical acid and base values for other fluids comparable as shown by Della Volpe and Siboni.[29,30] The

DOI: 10.1021/acsami.7b14311
ACS Appl. Mater. Interfaces XXXX, XXX, XXX−XXX

Table 1. LIS Experiments in This Work and Other Literature As Compared to the Model Prediction[a]

droplet	lubricant	coating/solid	experiment	prediction	predicted failure mode	ref
water	Krytox 1506	TFTS on Si pillars	yes	yes	N/A	17
toluene	Krytox 1506	TFTS on Si pillars	yes	yes	N/A	17
ethanol	Krytox 1506	TFTS on Si pillars	no	no	displacement of lubricant	17
octane	Krytox 1506	TFTS on Si pillars	yes	yes	N/A	17
hexane	Krytox 1506	TFTS on Si pillars	yes	yes	N/A	17
pentane	Krytox 1506	TFTS on Si pillars	yes	yes	N/A	17
perfluorohexane	Krytox 1506	TFTS on Si pillars	no	no	spreading of droplet	17
water	Krytox GPL 100	PTFE membrane	yes	yes	N/A	11
hexane	Krytox GPL 100	PTFE membrane	yes	no	displacement of lubricant	11
pentane	Krytox GPL 100	PTFE membrane	yes	no	displacement of lubricant	11
water	10 cSt Si oil	OTS on Si pillars	yes	yes	N/A	50
water	1000 cSt Si oil	OTS on Si pillars	yes	yes	N/A	50
water	Krytox GPL 101	TFTS on CuO nanoblades	yes	yes	N/A	b
water	5 cSt Si oil	TFTS on CuO nanoblades	yes	yes	N/A	b
water	ethanol	TFTS on CuO nanoblades	no	no	droplet and lubricant miscible	b
toluene	Krytox GPL 101	TFTS on CuO nanoblades	yes	yes	N/A	b
pentane	Krytox GPL 101	TFTS on CuO nanoblades	yes	yes	N/A	b

[a]The model predicted the experimental results with excellent accuracy, and also predicted the correct failure mode in the failed experimental cases. [b]Present work.

second concern may be addressed by choosing appropriate test fluids when characterizing the surface energy components,[31] or by choosing many fluids.[32,33] The final concern is assuaged by noting that negative surface energy component values reported are often of a lesser magnitude than the error of the measurement.[29,34] Even with the concerns addressed, there may still be significant error in prediction of interfacial energy over a broad range of fluids as pointed out by Kwok[35] and Lee.[36−38] In addition, in the specific case of LIS, a subset of prior work has used ionic liquids as lubricants; unfortunately, not only are there very limited data on the acid−base components of these liquids,[39−41] but the vOCG method would have trouble even with suitable data for pure ionic liquids due to the extent to which ionic liquids and water are mutually soluble, with water changing surface tension by nearly 50% in the presence of certain ionic liquids; therefore, ionic liquids are not considered in this analysis.[28,42] With these criticisms in mind, there is a wealth of literature on interfacial energy prediction,[43−47] including data for the vOCG LW, acid, and base components for over 150 fluids and solids compiled in the Supporting Information along with measurements taken in this study, and the consensus is that the vOCG method is the most versatile choice for a broad range of fluids.[27,28,30,34,48,49] Indeed, as demonstrated below, its predictive power is not only suitable for LIS, but it also offers additional insights that previously proposed design guidelines have not been able to properly capture.

RESULTS AND DISCUSSION

To test the validity of the proposed model, we performed experiments with several different combinations of impinging fluids and lubricants on a rough surface comprised of copper oxide (CuO) nanoblades fabricated on a copper tube substrate and subsequently functionalized with a low-surface-energy perfluorinated monolayer coating of trichloro(1*H*,1*H*,2*H*,2*H*-perfluorooctyl)silane (TFTS). The geometric factor for the CuO surface was $R = 0.80$, indicating that the surface was very rough. Water was used as the impinging fluid on LIS with lubricants of Krytox GPL 101 fluorinated oil, silicone oil (Shin Etsu 5 cSt), and ethanol on the functionalized CuO solid surface. With the Krytox GPL 101 fluorinated oil as a lubricant on the functionalized CuO surface, impinging fluids of toluene and pentane were also tested. The experiments were performed in a sealed environmental chamber. The LIS was first prepared by adding lubricant to the surface and removing excess lubricant with a nitrogen gun, and then the chamber was sealed and impinging fluid was condensed onto the LIS, which was chilled by a flow of controlled-temperature chiller fluid within the tube and observed with a video camera (see Experimental Design: Condensation Experiments). If discrete and mobile droplets were observed on the LIS exterior of the tube where the impinging fluid was condensing, the LIS configuration was deemed successful (see the Supporting Information).

For the combination of impinging fluid, lubricant, and solid surface used in each experiment, we also modeled the expected behavior using eqs 9−12 and the complete surface energy data for each fluid and solid presented in Table S1. Equations 9−12 must all be satisfied for the model to predict a successful LIS; if one or more of the equations were not satisfied, the failure mode predicted by the model was indicated in Table 1. The experimental results were compared with the model prediction in Table 1, where all of the experiments performed in the present work were in agreement with the model prediction. Interestingly, the model predicted not only the failure in the case with water impinging on the LIS of ethanol on CuO, but also the failure mechanism: criterion (V) was not satisfied, indicating that water and ethanol are miscible, which was the reason for the failure.

We also validated the model against experimental results in the literature. Rykaczewski et al. condensed water and low surface tension fluids on a LIS of Krytox 1506 oil infused in TFTS-coated silicon posts ($R = 0.76$) in a procedure similar to the present work.[17] They found that most of the configurations showed successful LIS promotion of droplet formation, but there were exceptions. In one case, the condensate (ethanol) displaced the lubricant; the model predicted failure in this case due to criterion (IV), where the strong polar interactions between the ethanol and the TFTS coating on the solid surface resulted in displacement of the Krytox oil. In another case,

DOI: 10.1021/acsami.7b14311
ACS Appl. Mater. Interfaces XXXX, XXX, XXX−XXX

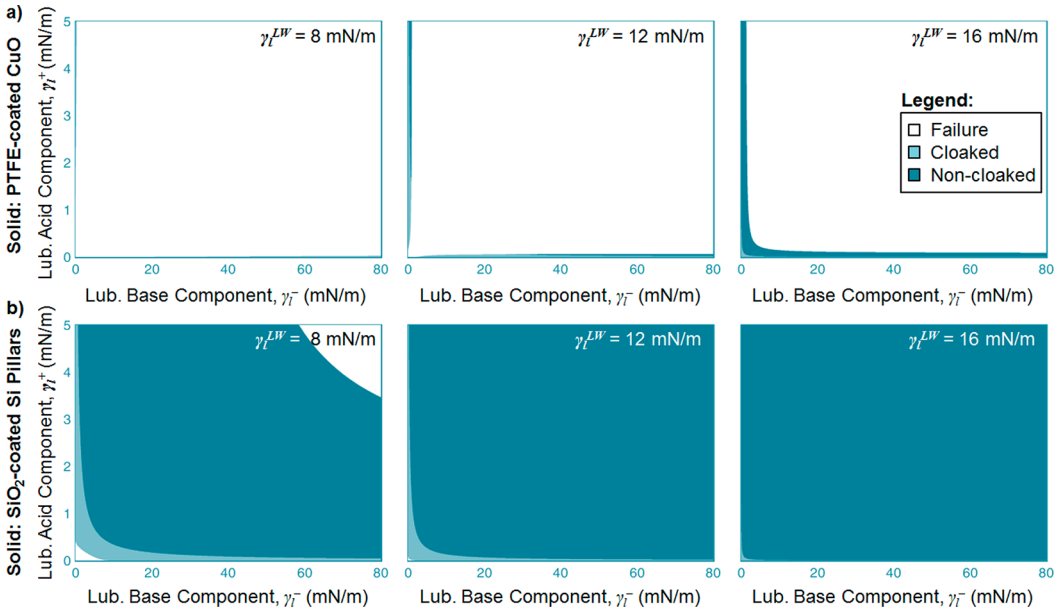

Figure 2. Parametric sweep of lubricant surface energy components γ_l^{LW}, γ_l^+, and γ_l^- on two different solid surfaces for a nonpolar impinging fluid with a surface tension of 17 mN/m. (a) A low-surface-energy surface of PTFE coated onto CuO nanoblades (R = 0.80) has no possible lubricant to design a LIS when γ_l^{LW} = 8, and the solution domain is limited to nonpolar fluids for higher values of γ_l^{LW}. (b) A high-surface-energy structured surface of SiO_2 pillars (R = 0.71) allows a much larger range of potential lubricants, including a wide range of potential lubricants which would allow noncloaked droplet formation (darker region).

Table 2. LIS Combinations Counterintuitive to Conventional Design Guidelines[a]

droplet	lubricant	solid/coating	I	II	III	IV	V	exp.	Figure
diiodomethane	methanol	bare SiO_2 pillars	no	yes	yes	yes	yes	yes	3A
(γ = 50.8 mN/m)	(γ = 22.5 mN/m)	(γ = 59.8 mN/m)							
(γ^{LW} = 50.8 mN/m)	(γ^{LW} = 18.2 mN/m)	(γ^{LW} = 42.0 mN/m)							
(γ^+ = 0.0 mN/m)	(γ^+ = 0.1 mN/m)	(γ^+ = 2.0 mN/m)							
(γ^- = 0.0 mN/m)	(γ^- = 77.0 mN/m)	(γ^- = 40.2 mN/m)							
methanol	diiodomethane	bare SiO_2 pillars	yes	no	yes	no	yes	no	3B
(γ = 22.5 mN/m)	(γ = 50.8 mN/n)	(γ = 59.8 mN/m)							
(γ^{LW} = 18.2 mN/m)	(γ^{LW} = 50.8 mN/m)	(γ^{LW} = 42.0 mN/m)							
(γ^+ = 0.1 mN/m)	(γ^+ = 0.0 mN/m)	(γ^+ = 2.0 mN/m)							
(γ^- = 77.0 mN/m)	(γ^- = 0.0 mN/m)	(γ^- = 40.2 mN/m)							
heptane	methanol	bare SiO_2 pillars	yes	yes	yes	yes	yes	yes	3C
(γ = 20.1 mN/m)	(γ = 22.5 mN/n)	(γ = 59.8 mN/m)							
(γ^{LW} = 20.1 mN/m)	(γ^{LW} = 18.2 mN/m)	(γ^{LW} = 42.0 mN/m)							
(γ^+ = 0.0 mN/m)	(γ^+ = 0.1 mN/m)	(γ^+ = 2.0 mN/m)							
(γ^- = 0.0 mN/m)	(γ^- = 77.0 mN/m)	(γ^- = 40.2 mN/m)							
butane	hexafluoro-IPA	bare SiO_2 pillars	yes	yes	yes	yes	yes	yes	4
(γ = 12.5 mN/m)	(γ = 14.7 mN/m)	(γ = 59.8 mN/m)							
(γ^{LW} = 12.5 mN/m)	($\gamma^{LW} \approx$ 10.4 mN/m)	(γ^{LW} = 42.0 mN/m)							
(γ^+ = 0.0 mN/m)	($\gamma^+ \approx$ 0.0 mN/m)	(γ^+ = 2.0 mN/m)							
(γ^- = 0.0 mN/m)	($\gamma^- \approx$ 70.0 mN/m)	(γ^- = 40.2 mN/m)							

[a]The impinging droplet, lubricant, and solid/coating are described along with their relevant surface energy components. The model prediction for criteria I–V is shown to the right, and the experiment success or failure is indicated.

perfluorohexane spread over the LIS, which was also accurately captured as the failure mode by the model when criterion (II) was not met. Wong placed droplets onto a PTFE membrane (estimated R = 0.82) infused with Krytox GPL 100 oil;[11] in this study, all of the experiments were successful. Finally, Anand condensed water onto a LIS of silicone oil (viscosities of 10 and 1000 cSt) infused in silicon pillars (R = 0.57) coated with octadecyltrichlorosilane (OTS),[50] where again all of the experiments were successful.

Through comparison of the model with 17 total experimental cases, 5 from the present study and 12 from literature, we found that the model had predicted success or failure of the LIS with nearly 90% accuracy. Of equal importance, in each of the failure cases considered, the model revealed why the failure occurred. With this in mind, we proceeded to use the model to explore the validity of some common guidelines proposed in the LIS field. First, we explored whether the solid must have a low surface energy.[50] Our model indicates that the solid need not have a low surface energy; in fact, the opposite case appears to

DOI: 10.1021/acsami.7b14311
ACS Appl. Mater. Interfaces XXXX, XXX, XXX−XXX

be more desirable in some scenarios. Figure 2 shows a parametric sweep of the three surface energy components (LW, acid, and base) of the lubricant for two different solids, a low-surface-energy PTFE-coated solid in Figure 2a and a high-surface-energy SiO_2-coated solid in Figure 2b, with the goal of repelling a nonpolar impinging fluid with surface tension 17 mN/m. The range of feasible lubricants for the SiO_2 solid surface is much more expansive, including (1) providing possible solutions for γ_l^{LW} = 8 mN/m when the PTFE-coated surface provides none and (2) providing a much larger margin of error to avoid droplet cloaking in all cases by introducing acid−base components to the lubricant and entering the large noncloaking regions (darker shaded regions). (Note that the model indicates that a nonpolar fluid with surface tension of 16 mN/m is a suitable lubricant for an impinging nonpolar fluid with surface tension of 17 mN/m, which raises concerns about the accuracy of the miscibility criterion (V); the effect of a more conservative miscibility criterion is discussed in the Supporting Information.)

We experimentally tested a LIS with a high-surface-energy solid by using plasma-cleaned SiO_2-coated silicon pillars. These SiO_2-coated pillars were fabricated on a silicon wafer, and as such were not able to be applied to the cylindrical exterior of our condenser tubes as used in the previously described experimental setup. We characterized the LIS in this case with a droplet impingement experiment, described in detail in the Supporting Information. Note that the droplet impingement was performed at a near-zero impact velocity; as a result, fluid hammer pressure and dynamic effects were not significant. As shown in Table 2, the model predicted that methanol could be a suitable lubricant for the impinging fluids diiodomethane and heptane. This is primarily due to the strong Lewis acid−base polar interaction between methanol and SiO_2, which helps to satisfy criteria (III) and (IV). Figure 3a and c show the experimental results in these two cases for a droplet impinging on an inclined surface of SiO_2 pillars infused with methanol (see Experimental Design: Droplet Impingement Experiments). The sequence of frames from left to right shows highly mobile discrete droplets of both diiodomethane and heptane form on the LIS of methanol in SiO_2 pillars, indicating a successful LIS in agreement with the model prediction and demonstrating a LIS that utilizes a high-surface-energy solid material in contrast with past work, which has relied on low-surface-energy solids. This is particularly useful for future LIS design because thin, low-surface-energy coatings often lack durability;[20] we demonstrate here that these coatings are not necessary for LIS.

Even more intriguing is the consideration of whether LIS can be used to promote droplet formation for impinging fluids with surface tensions below the critical surface energy of the solid.[17] Certainly droplets will not form for a fluid impinging directly onto a solid if the fluid has a surface tension lower than the solid's relevant critical surface energy by definition. However, our model predicts that a suitably designed LIS can promote formation of droplets with finite wetting angle even when the impinging fluid has a surface energy lower than that of the solid surface. Specifically, we have chosen the example of SiO_2 pillars with methanol as the lubricating fluid and heptane as the impinging fluid, where the lowest reported critical surface tension of SiO_2 is 27.7 mN/m[51,52] and the surface tension of heptane is 20.1 mN/m. In this case, the model predicts that all of the criteria (I)−(V) will be satisfied. Criteria (III) and (IV) are once again satisfied due to the strong polar affinity between methanol and SiO_2. The model also predicts that eq 13 will be satisfied to avoid both droplet cloaking and spreading of the nonpolar impinging fluid; this is possible due to methanol having a lower LW component of surface energy than heptane while also having a sufficiently large polar component of surface energy. The results of the experiment with this LIS configuration are shown in Figure 3c, where discrete and mobile droplets of heptane form on the methanol/SiO_2 LIS in agreement with the model prediction. This demonstration indicates that the LIS enables formation of discrete droplets on a solid surface with a critical surface energy higher than that of the impinging droplets, so long as an appropriate lubricating fluid is chosen.

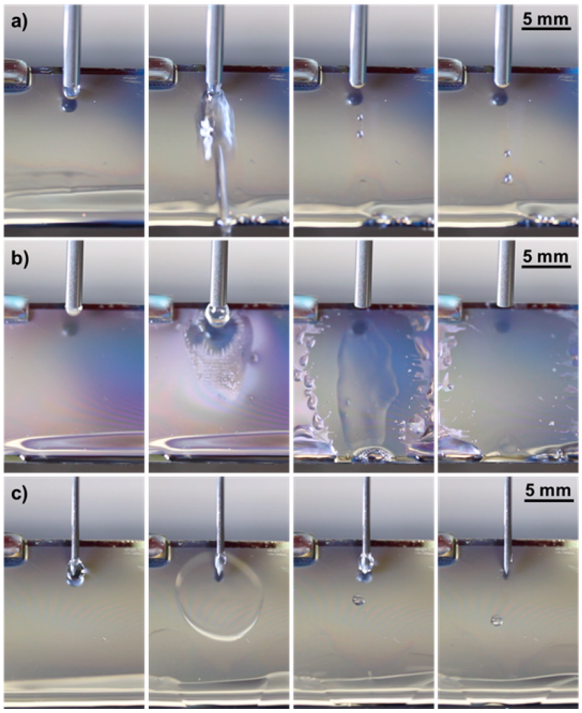

Figure 3. Experimental results from droplet impingement tests for counterintuitive LIS designs. The first frame of each sequence shows the droplet attached to the syringe before impingement. (a) Diiodomethane is dropped onto a LIS of methanol infused in SiO_2 pillars. Discrete, mobile droplets of diiodomethane form on the LIS and roll down the surface. (b) Methanol is dropped onto a LIS of diiodomethane infused in SiO_2 pillars. The methanol forces the diiodomethane lubricant out of the SiO_2 pillars as predicted by the model. The interface between methanol and diiodomethane is observed propagating outward from the initial impingement site in the second image in the sequence, and by the final image in the sequence the diiodomethane is completely displaced. (c) Heptane is dropped onto a LIS of methanol infused in SiO_2 pillars. Discrete droplets of heptane form and slide down the LIS even though the surface tension of heptane is lower than the critical surface energy of SiO_2, indicating that LIS allows droplet formation on a solid with a critical surface energy higher than the impinging fluid so long as an appropriate lubricant is chosen.

We also considered whether the lubricating fluid should have a surface tension similar to that of the solid surface.[53] We already know from the experiment shown in Figure 3a that methanol is a suitable lubricant for the SiO_2 solid surface despite having an overall surface energy of less than 40% that of SiO_2. We considered the reverse case, where methanol was taken as the impinging fluid and diiodomethane, with a better "matching" surface energy 85% that of SiO_2, was taken as the

DOI: 10.1021/acsami.7b14311
ACS Appl. Mater. Interfaces XXXX, XXX, XXX−XXX

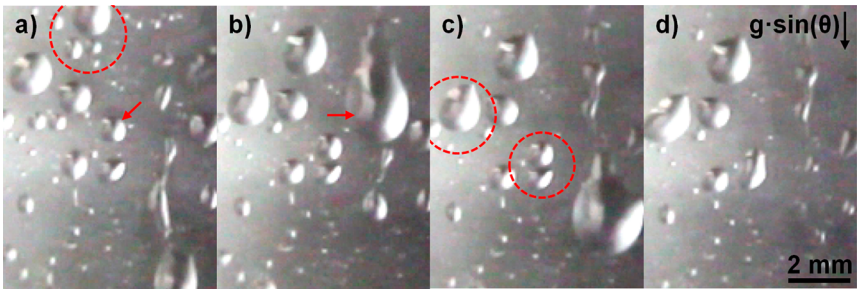

Figure 4. Behavior of liquid butane impinging on a LIS of 6F-IPA infused in silicon micropillars. The experiment was performed inside of a glass vial at elevated pressure. Photos a–d are time lapse images of droplets moving on the LIS after being sprayed on the surface. The dashed red circles indicate when droplet coalescence events are about to occur, and the red arrows indicate droplets sliding on the surface, which occur at approximately the capillary length (1.4 mm) in this case. Droplets of butane deposited onto a flat SiO_2 surface in the same experimental setup immediately spread over the surface.

lubricant. In this case, the model predicted that the strong polar affinity between the methanol and the SiO_2 would not allow criterion (IV) to be satisfied and would consequently result in forced dewetting of the diiodomethane from the SiO_2 pillars even though the diiodomethane has a surface energy much more closely matched to that of the SiO_2. The experimental result from the droplet impingement test is shown in Figure 3b, where the diiodomethane is indeed forced out of the SiO_2 pillars by the methanol with the interface between the two observed propagating away from the impingement site until the diiodomethane is completely displaced. This result demonstrates that the overall surface energies of the lubricant and the solid surface need not necessarily match.

Finally, we took advantage of the potential for a strong polar interaction between the lubricant and a high-surface-energy solid to design a LIS to repel extremely low surface tension impinging fluids. Previously, multiple reports have indicated that LIS are able to repel pentane ($\gamma \approx 17$ mN/m),[11,17] but lower surface tension fluids such as perfluorohexane ($\gamma \approx 11$ mN/m) could not be repelled. We used the same SiO_2 pillared solid surface as in the experiments shown in Figure 3, but we chose hexafluoroisopropanol (6F-IPA) as the lubricant to maintain the strong polar interaction through the presence of its −OH group while simultaneously exhibiting a significantly lower LW component of surface energy as compared to methanol due to the fluorination. The model predicted that this surface would be able to repel nonpolar impinging fluids with surface tensions as low as ∼11 mN/m; we performed an experiment with butane ($\gamma \approx 13$ mN/m) as the impinging fluid. We modified the experimental setup by placing it inside a glass vial to accommodate butane's superatmospheric vapor pressure (∼2.5 atm) at standard temperature, which resulted in a limited field of view. We first performed a control experiment during which we sprayed droplets of butane onto a flat plasma-cleaned SiO_2 surface and found that butane droplets impinging onto the flat SiO_2 surface spread completely, as expected due to the surface tension of butane being lower than the critical surface energy of SiO_2. We then sprayed butane droplets onto the proposed LIS of 6F-IPA infused into the SiO_2 pillars, with the result shown in Figure 4. Discrete droplets formed on the surface, and the droplets exhibited a high degree of mobility as well as typical droplet behavior such as multiple sweeping and coalescence events.

The energy-based analysis presented in this work is useful in eliminating combinations of impinging fluid, lubricant, and solid surface that are guaranteed to fail, but prediction of a successful LIS with our model does not guarantee desired performance in every application. It is possible in certain applications that other criteria must also be met for a successful LIS. For example, when repelling high-speed impinging droplets, the fluid hammer pressure and dynamic droplet behavior must be accounted for.[54] In applications involving flow of an impinging fluid over the LIS, shear at the impinging fluid–lubricant interface may result in lubricant depletion as lubricant is forced out of the structured surface.[2] In any open system, evaporation of the lubricant from the surface over extended periods of time may also be a concern. Gravity may even drive lubricant depletion for large enough surfaces (see discussion in the Supporting Information). Fortunately, the fundamental understanding of surface energetics presented here offers an excellent starting point for the design of any lubricant infused surface.

CONCLUSION

We developed a model that predicts interfacial surface energies to determine whether an arbitrary combination of solid and lubricant will repel a given impinging fluid. This model was validated against experiments performed in the present work as well as the literature and subsequently used to develop a new framework for LIS design and provide unique design guidelines. Furthermore, we demonstrated LIS on uncoated high-surface-energy solids, eliminating the need for unreliable low-surface-energy coatings. The vOCG-based approach to LIS design using high-surface-energy solids and polar lubricants resulted in repulsion of discrete droplets of the lowest surface tension fluid recorded to date (butane, $\gamma \approx 13$ mN/m). This demonstration of LIS repelling extremely low-surface-tension fluids is promising for applications in thermal management[14,55] and hydrocarbon processing.[17] More broadly, the insights gained from the vOCG framework will promote new developments in LIS design, paving the way for new technology in biological science, lab-on-a-chip, thermofluidics, and beyond.

MATERIALS AND METHODS

Experimental Design: Condensation Experiments. Condensation experiments were performed inside of a controlled environmental chamber. TFTS-functionalized CuO coatings were applied to the exterior surface of copper condenser tubes.[56] The TFTS-coated CuO was infused with lubricant by first placing a few droplets of lubricant onto the surface and allowing them to spread completely, then using a nitrogen stream (99.9%, Airgas) to shear off excess lubricant. Following the addition of lubricant, the chamber was sealed and noncondensable gases were evacuated with a vacuum pump (except in the case of the ethanol lubricant, where the vacuum pump was not used so as not to evaporate the ethanol). Pure vapor of the impinging

DOI: 10.1021/acsami.7b14311
ACS Appl. Mater. Interfaces XXXX, XXX, XXX–XXX

condensate was then introduced as the tube sample was cooled from within with a chiller loop set to 15 °C. The behavior of the condensate was imaged from a viewport during condensation.

Experimental Design: Droplet Impingement Experiments. Droplet impingement experiments were performed with the LIS held at ∼45° from horizontal inside of a fume hood. Excess lubricant was added to the base of the dry, plasma cleaned[57] SiO_2 pillar structured surface and allowed to wick into the SiO_2 pillars until they were filled with lubricant. The droplets of the impinging fluid were then dispensed from a syringe with a stainless steel needle. Images were taken at an angle of ∼0° from horizontal with a camera outside of the hood. For the experiment with butane as the impinging fluid, to prevent rapid evaporation of butane, the LIS was placed inside of a glass vial, infused with the 6F-IPA, and then a small amount of butane was placed at the bottom of the vial and the vial was sealed and allowed to reach saturation conditions. Butane droplets were then introduced through a port at the top of the vial.

Pendant Drop Measurements. The surface energy components were determined for Krytox oil using the pendant drop method to characterize the interfacial tension of Krytox oil with multiple test liquids including water, ethylene glycol, glycerol, 1-bromonapthalene, and chloroform. The pendant drop measurement system consisted of a collimated light source (Thorlabs 6500 K, 440 mW Collimated LED) illuminating the droplet and aligned with a telecentric lens (Edmund 0.25X SilverTL) attached to a camera (PointGrey CM3-U3-13Y3C) capturing images. The droplets were dispensed with a Harvard Apparatus syringe pump through stainless steel needles, and when interfacial tension between two fluids was measured, the second fluid was contained inside of a glass cuvette. Glass cuvettes were cleaned thoroughly with Alconox followed by progressive solvent rinses in acetone, methanol, ethanol, isopropanol, and finally 99.99% pure DI water, and then nitrogen stream drying (99.9%, Airgas). Interfacial tensions were characterized from images using a plugin for ImageJ.[58] The surface energy components were determined from a plane fit to the data based on the vOCG equations, detailed in the Supporting Information.

Surface Fabrication. To create the CuO nanostructures, commercially available oxygen-free Cu tubes (99.9% purity) with outer diameters D_{OD} = 6.35 mm, inner diameters D_{ID} = 3.56 mm, and lengths L = 131 mm, were used. Each Cu tube was cleaned in an ultrasonic bath with acetone for 10 min and rinsed with ethanol, isopropanol, and deionized (DI) water. The tubes were then dipped into a 2.0 M hydrochloric acid solution for 10 min to remove the native oxide film on the surface, then triple-rinsed with DI water and dried with clean nitrogen gas. Nanostructured CuO films were formed by immersing the cleaned tubes (with ends capped) into a hot (96 ± 3 °C) alkaline solution composed of $NaClO_2$, NaOH, $Na_3PO_4{\cdot}12H_2O$, and DI water (3.75:5:10:100 wt %).[59−62] During the oxidation process, a thin (∼300 nm) Cu_2O layer was formed that then reoxidized to form sharp, knife-like CuO structures with heights of $h \approx 1\ \mu m$, solid fraction $\varphi \approx 0.038$, and roughness factor $r \approx 4$.

Silicon micropillar surfaces (Figure 4d) with diameters of $d = 7\ \mu m$, heights of $h = 20\ \mu m$, and center-to-center spacings of $l = 20\ \mu m$ (solid fraction $\varphi = \pi d^2/4l^2 = 0.096$ and roughness factor $r = 1 + \pi dh/l^2 = 3.20$) were fabricated using projection lithography and deep reactive ion etching.

Surface Functionalization. Trichloro(1*H*,1*H*,2*H*,2*H*-perfluorooctyl)silane (TFTS) (Sigma-Aldrich) was deposited from the vapor phase. Prior to silane deposition, each tube was oxygen plasma cleaned for 2 h to remove organic contaminants on the surface. Once clean, the tube samples were immediately placed in a vacuum desiccator (06514-10, Cole Parmer) with a small amount of liquid TFTS. The desiccator was evacuated by a roughing pump for 2 min to a minimum pressure of ∼2 kPa. A valve was then closed to isolate the pump from the desiccator, and the sample was held in a vacuum (∼ 2 kPa) for another 10 min. The functionalized surfaces were then rinsed in ethanol and DI water and dried in a clean nitrogen stream. The coating had a typical water advancing contact angle of $\theta_a \approx 120°$ when measured on a smooth reference surface and typical water advancing/receding contact angles of $\theta_a/\theta_r \approx 171/167 \pm 3°$ when measured on the nanostructured CuO surface.

■ ASSOCIATED CONTENT

Supporting Information

The Supporting Information is available free of charge on the ACS Publications website at DOI: 10.1021/acsami.7b14311.

Tabulated surface energy components for 167 fluids and solids; method for experimental determination of surface energy components; discussion on surface geometry, fluid miscibility constraint, and choice of solid material for polar impinging fluids; results from condensation experiments; details on droplet impingement experimental setup; discussion on reduction in number of required experiments using vOCG method; and analysis of effects of gravity (PDF)

■ AUTHOR INFORMATION

Corresponding Author

*E-mail: enwang@mit.edu.

ORCID

Daniel J. Preston: 0000-0002-0096-0285

Zhengmao Lu: 0000-0002-5938-717X

Author Contributions

D.J.P. and E.N.W. conceived the idea. D.J.P., Y.S., and Z.L. developed the model. D.J.P., Y.S., and D.S.A. performed the experimental analysis. E.N.W. guided the work.

Notes

The authors declare no competing financial interest.

■ ACKNOWLEDGMENTS

We gratefully acknowledge funding support from the Abu Dhabi National Oil Co. (ADNOC) with Dr. Abdullah Al Mahri as program manager and from the Office of Naval Research (ONR) with Dr. Mark Spector as program manager. D.J.P. acknowledges funding received by the National Science Foundation Graduate Research Fellowship under grant no. 1122374. Any opinion, findings, conclusions, or recommendations expressed in this material are those of the authors(s) and do not necessarily reflect the views of the National Science Foundation. D.S.A. and E.N.W. acknowledge funding from the Electric Power Research Institute (EPRI) under award number 00-10002062. Y.S. acknowledges funding received from Exelon Corp. Z.L. acknowledges funding from the Air Force Office of Scientific Research (AFOSR) with Dr. Ali Sayir as program manager. This work was performed in part at the Center for Nanoscale Systems (CNS), a member of the National Nanotechnology Infrastructure Network (NNIN), which is supported by the National Science Foundation under NSF award no. ECS-0335765. CNS is part of Harvard University.

■ REFERENCES

(1) Kim, P.; Kreder, M. J.; Alvarenga, J.; Aizenberg, J. Hierarchical or Not? Effect of the Length Scale and Hierarchy of the Surface Roughness on Omniphobicity of Lubricant-Infused Substrates. *Nano Lett.* **2013**, *13* (4), 1793−1799.

(2) Wexler, J. S.; Jacobi, I.; Stone, H. A. Shear-Driven Failure of Liquid-Infused Surfaces. *Phys. Rev. Lett.* **2015**, *114* (16), 168301−168305.

(3) Irajizad, P.; Hasnain, M.; Farokhnia, N.; Sajadi, S. M.; Ghasemi, H. Magnetic slippery extreme icephobic surfaces. *Nat. Commun.* **2016**, *7*, 13395.

(4) Park, K. C.; Kim, P.; Grinthal, A.; He, N.; Fox, D.; Weaver, J. C.; Aizenberg, J. Condensation on slippery asymmetric bumps. *Nature* **2016**, *531* (7592), 78−82.
(5) Epstein, A. K.; Wong, T. S.; Belisle, R. A.; Boggs, E. M.; Aizenberg, J. Liquid-infused structured surfaces with exceptional anti-biofouling performance. *Proc. Natl. Acad. Sci. U. S. A.* **2012**, *109* (33), 13182−13187.
(6) Boreyko, J. B.; Polizos, G.; Datskos, P. G.; Sarles, S. A.; Collier, C. P. Air-stable droplet interface bilayers on oil-infused surfaces. *Proc. Natl. Acad. Sci. U. S. A.* **2014**, *111* (21), 7588−7593.
(7) Vaaler, L. E. Impregnated porous condenser surfaces. U.S. Patent 2919115, 1959.
(8) Verheijen, H. J. J.; Prins, M. W. J. Reversible electrowetting and trapping of charge: Model and experiments. *Langmuir* **1999**, *15* (20), 6616−6620.
(9) Quere, D. Non-sticking drops. *Rep. Prog. Phys.* **2005**, *68* (11), 2495−2532.
(10) Lafuma, A.; Quere, D. Slippery pre-suffused surfaces. *Epl-Europhys. Lett.* **2011**, *96* (5), 56001.
(11) Wong, T. S.; Kang, S. H.; Tang, S. K. Y.; Smythe, E. J.; Hatton, B. D.; Grinthal, A.; Aizenberg, J. Bioinspired self-repairing slippery surfaces with pressure-stable omniphobicity. *Nature* **2011**, *477* (7365), 443−447.
(12) Xiao, R.; Miljkovic, N.; Enright, R.; Wang, E. N. Immersion Condensation on Oil-Infused Heterogeneous Surfaces for Enhanced Heat Transfer. *Sci. Rep.* **2013**, *3*, 1988.
(13) Miljkovic, N.; Xiao, R.; Preston, D. J.; Enright, R.; McKay, I.; Wang, E. N. Condensation on Hydrophilic, Hydrophobic, Nano-structured Superhydrophobic and Oil-Infused Surfaces. *J. Heat Transfer* **2013**, *135* (8), 080906.
(14) Cho, H. J.; Preston, D. J.; Zhu, Y.; Wang, E. N. Nano-engineering materials for liquid−vapour phase-change heat transfer. *Nature Materials Reviews* **2016**, *2*, 16092.
(15) Kim, P.; Wong, T. S.; Alvarenga, J.; Kreder, M. J.; Adorno-Martinez, W. E.; Aizenberg, J. Liquid-Infused Nanostructured Surfaces with Extreme Anti-Ice and Anti-Frost Performance. *ACS Nano* **2012**, *6* (8), 6569−6577.
(16) Glavan, A. C.; Martinez, R. V.; Subramaniam, A. B.; Yoon, H. J.; Nunes, R. M. D.; Lange, H.; Thuo, M. M.; Whitesides, G. M. Omniphobic "R-F Paper" Produced by Silanization of Paper with Fluoroalkyltrichlorosilanes. *Adv. Funct. Mater.* **2014**, *24* (1), 60−70.
(17) Rykaczewski, K.; Paxson, A. T.; Staymates, M.; Walker, M. L.; Sun, X. D.; Anand, S.; Srinivasan, S.; McKinley, G. H.; Chinn, J.; Scott, J. H. J.; Varanasi, K. K. Dropwise condensation of low surface tension fluids on omniphobic surfaces. *Sci. Rep.* **2015**, *4*, 4158.
(18) Smith, D. J.; Dhiman, R.; Anand, S.; Reza-Garduno, E.; Cohen, R. E.; McKinley, G. H.; Varanasi, K. K. Droplet mobility on lubricant-impregnated surfaces. *Soft Matter* **2013**, *9*, 1772−1780.
(19) van Oss, C. J.; Chaudhury, M. K.; Good, R. J. Interfacial Lifshitz-Vanderwaals and Polar Interactions in Macroscopic Systems. *Chem. Rev.* **1988**, *88* (6), 927−941.
(20) Preston, D. J.; Mafra, D. L.; Miljkovic, N.; Kong, J.; Wang, E. N. Scalable graphene coatings for enhanced condensation heat transfer. *Nano Lett.* **2015**, *15* (5), 2902−2909.
(21) Fowkes, F. M. Attractive Forces at Interfaces. *Ind. Eng. Chem.* **1964**, *56* (12), 40−52.
(22) Fowkes, F. M. Determination of Interfacial Tensions, Contact Angles, and Dispersion Forces in Surfaces by Assuming Additivity of Intermolecular Interactions in Surfaces. *J. Phys. Chem.* **1962**, *66* (2), 382.
(23) Owens, D. K.; Wendt, R. C. Estimation of Surface Free Energy of Polymers. *J. Appl. Polym. Sci.* **1969**, *13* (8), 1741−1747.
(24) van Oss, C. J.; Good, R. J. Prediction of the Solubility of Polar Polymers by Means of Interfacial-Tension Combining Rules. *Langmuir* **1992**, *8* (12), 2877−2879.
(25) van Oss, C. J.; Good, R. J. On the Mechanism of Hydrophobic Interactions. *J. Dispersion Sci. Technol.* **1988**, *9* (4), 355−362.
(26) Aria, A. I.; Kidambi, P. R.; Weatherup, R. S.; Xiao, L.; Williams, J. A.; Hofmann, S. Time Evolution of the Wettability of Supported Graphene under Ambient Air Exposure. *J. Phys. Chem. C* **2016**, *120* (4), 2215−2224.
(27) Kontogeorgis, G. M.; Kiil, S. *Introduction to Applied Colloid and Surface Chemistry*; John Wiley & Sons: New York, 2016.
(28) Janczuk, B.; Wojcik, W.; Zdziennicka, A. Determination of the Components of the Surface-Tension of Some Liquids from Interfacial Liquid-Liquid Tension Measurements. *J. Colloid Interface Sci.* **1993**, *157* (2), 384−393.
(29) Della Volpe, C.; Siboni, S. Some reflections on acid-base solid surface free energy theories. *J. Colloid Interface Sci.* **1997**, *195* (1), 121−136.
(30) Della Volpe, C.; Maniglio, D.; Brugnara, M.; Siboni, S.; Morra, M. The solid surface free energy calculation - I. In defense of the multicomponent approach. *J. Colloid Interface Sci.* **2004**, *271* (2), 434−453.
(31) Della Volpe, C.; Siboni, S. Acid-base surface free energies of solids and the definition of scales in the Good-van Oss-Chaudhury theory. *J. Adhes. Sci. Technol.* **2000**, *14* (2), 235−272.
(32) Fernandez, V.; Khayet, M. Evaluation of the surface free energy of plant surfaces: toward standardizing the procedure. *Front. Plant Sci.* **2015**, *6*, 510.
(33) Dalal, E. N. Calculation of Solid-Surface Tensions. *Langmuir* **1987**, *3* (6), 1009−1015.
(34) Weng, M.; Shen, Q. Effect of liquid surface tension data on the validity and accuracy of solid surface tension components and parameters in the application of the van Oss-Chaudhury-Good approach. *J. Adhes. Sci. Technol.* **2014**, *28* (22−23), 2248−2268.
(35) Kwok, D. Y. The usefulness of the Lifshitz-van der Waals/acid-base approach for surface tension components and interfacial tensions. *Colloids Surf., A* **1999**, *156* (1−3), 191−200.
(36) Lee, L. H. Relevance of film pressures to interfacial tension, miscibility of liquids, and Lewis acid-base approach. *J. Colloid Interface Sci.* **1999**, *214* (1), 64−78.
(37) Lee, L. H. The gap between the measured and calculated liquid-liquid interfacial tensions derived from contact angles. *J. Adhes. Sci. Technol.* **2000**, *14* (2), 167−185.
(38) Lee, L. H. The unified Lewis acid-base approach to adhesion and solvation at the liquid-polymer interface. *J. Adhes.* **2001**, *76* (2), 163−183.
(39) Restolho, J.; Mata, J. L.; Saramago, B. On the interfacial behavior of ionic liquids: Surface tensions and contact angles. *J. Colloid Interface Sci.* **2009**, *340* (1), 82−86.
(40) Law, G.; Watson, P. R. Surface tension measurements of N-alkylimidazolium ionic liquids. *Langmuir* **2001**, *17* (20), 6138−6141.
(41) Tariq, M.; Freire, M. G.; Saramago, B.; Coutinho, J. A. P.; Lopes, J. N. C.; Rebelo, L. P. N. Surface tension of ionic liquids and ionic liquid solutions. *Chem. Soc. Rev.* **2012**, *41* (2), 829−868.
(42) Anand, S.; Paxson, A. T.; Dhiman, R.; Smith, D. J.; Varanasi, K. K. Enhanced condensation on lubricant-impregnated nanotextured surfaces. *ACS Nano* **2012**, *6* (11), 10122−10129.
(43) Clint, J. H. Adhesion and components of solid surface energies. *Curr. Opin. Colloid Interface Sci.* **2001**, *6* (1), 28−33.
(44) van Oss, C. J.; Wu, W.; Docoslis, A.; Giese, R. F. The interfacial tensions with water and the Lewis acid-base surface tension parameters of polar organic liquids derived from their aqueous solubilities. *Colloids Surf., B* **2001**, *20* (1), 87−91.
(45) Boudenne, A.; Ibos, L.; Candau, Y.; Thomas, S. Handbook of Multiphase Polymer Systems. *Handbook of Multiphase Polymer Systems* **2011**, *1*−*2*, 1−1010.
(46) Peterson, I. R. Towards a theory of adhesion with predictive power. *Surf. Coat. Int., Part B* **2005**, *88* (1), 1−8.
(47) Chaudhury, M. K. Interfacial interaction between low-energy surfaces. *Mater. Sci. Eng., R* **1996**, *16* (3), 97−159.
(48) Xu, Z. H.; Liu, Q. X.; Ling, J. H. An Evaluation of the Van Oss-Chaudhury-Good Equation and Neumanns Equation of State Approach with Mercury Substrate. *Langmuir* **1995**, *11* (3), 1044−1046.

DOI: 10.1021/acsami.7b14311
ACS Appl. Mater. Interfaces XXXX, XXX, XXX−XXX

(49) Gardner, D. J. Application of the Lifshitz-van der Waals acid-base approach to determine wood surface tension components. *Wood Fiber Sci.* **1996**, *28*, 422−428.
(50) Anand, S.; Rykaczewski, K.; Subramanyam, S. B.; Beysens, D.; Varanasi, K. K. How droplets nucleate and grow on liquids and liquid impregnated surfaces. *Soft Matter* **2015**, *11* (1), 69−80.
(51) Thomas, R. R.; Kaufman, F. B.; Kirleis, J. T.; Belsky, R. A. Wettability of polished silicon oxide surfaces. *J. Electrochem. Soc.* **1996**, *143* (2), 643−648.
(52) Gould, G.; Irene, E. A. An Insitu Study of Aqueous Hf Treatment of Silicon by Contact-Angle Measurement and Ellipsometry. *J. Electrochem. Soc.* **1988**, *135* (6), 1535−1539.
(53) Aizenberg, J.; Aizenberg, M.; Kim, P. Slips Surface Based on Metal-Containing Compound. U.S. Patent Application US20150175814 A1, 2015.
(54) Lee, C.; Kim, H.; Nam, Y. Drop Impact Dynamics on Oil-Infused Nanostructured Surfaces. *Langmuir* **2014**, *30* (28), 8400−8407.
(55) Jung, S. M.; Preston, D. J.; Jung, H. Y.; Deng, Z. T.; Wang, E. N.; Kong, J. Porous Cu nanowire aerosponges from one-step assembly and their applications in heat dissipation. *Adv. Mater.* **2016**, *28* (7), 1413−1419.
(56) Bhatia, B.; Preston, D. J.; Bierman, D. M.; Miljkovic, N.; Lenert, A.; Enright, R.; Nam, Y.; Lopez, K.; Dou, N.; Sack, J.; Chan, W. R.; Celanovic, I.; Soljacic, M.; Wang, E. N. Nanoengineered Surfaces for Thermal Energy Conversion. *15th International Conference on Micro and Nanotechnology for Power Generation and Energy Conversion Applications (Powermems 2015)* 2015; Vol. *660*, p 012036.
(57) Preston, D. J.; Miljkovic, N.; Sack, J.; Enright, R.; Queeney, J.; Wang, E. N. Effect of hydrocarbon adsorption on the wettability of rare earth oxide ceramics. *Appl. Phys. Lett.* **2014**, *105*, 011601.
(58) Daerr, A.; Mogne, A. Pendent_Drop: An ImageJ Plugin to Measure the Surface Tension from an Image of a Pendent Drop. *J. Open Res. Software* **2016**, *4*, 3.
(59) Nam, Y.; Ju, Y. S. Comparative Study of Copper Oxidation Schemes and Their Effects on Surface Wettability. *Imece 2008: Heat Transfer, Fluid Flows, and Thermal Systems* **2009**, *10*, 1833−1838.
(60) Preston, D. J.; Anders, A.; Barabadi, B.; Tio, E.; Zhu, Y.; Dai, D. A.; Wang, E. N. Electrowetting-on-dielectric actuation of a vertical translation and angular manipulation stage. *Appl. Phys. Lett.* **2016**, *109* (24), 244102.
(61) Preston, D. J.; Anders, A.; Barabadi, B.; Tio, E.; Zhu, Y.; Dai, D. A.; Wang, E. N. Electrowetting-on-dielectric actuation of a spatial and angular manipulation MEMS stage. *2017 IEEE 30th International Conference on Micro Electro Mechanical Systems (MEMS)*; IEEE: Las Vegas, NV, 2017; pp 769−772.
(62) Preston, D. J.; Miljkovic, N.; Enright, R.; Wang, E. N. Jumping droplet electrostatic charging and effect on vapor drag. *J. Heat Transfer* **2014**, *136* (8), 080909.

DOI: 10.1021/acsami.7b14311
ACS Appl. Mater. Interfaces XXXX, XXX, XXX−XXX

Supporting Information:

Design of Lubricant Infused Surfaces

Daniel J. Preston, Youngsup Song, Zhengmao Lu, Dion S. Antao, and Evelyn N. Wang*

Department of Mechanical Engineering, Massachusetts Institute of Technology, Cambridge, Massachusetts 02139, USA

**Corresponding author email: enwang@mit.edu*

S1. vOCG Surface Energy Components

Table S1. Compilation of vOCG surface energy components for 167 fluids and solids at room temperature and atmospheric pressure.

Fluid/Solid	γ (mN/m)	γ^{LW} (mN/m)	γ^{AB} (mN/m)	γ^{+} (mN/m)	γ^{-} (mN/m)	SI Ref.
Benzene	28.9	28.9	0	0	0.96	[1]
Chlorobenzene	33.6	32.1	1.5	0.9	0.61	[2]
Chloroform	27.2	27.2	0	1.5	0	[3]
Cyclohexane	25.24	25.24	0	0	0	[2]
cis-Decahydrohaphthalene	32.2	32.2	0	0	0	[3]
Decane	23.83	23.83	0	0	0	[2]
Diethyl Ether (ethoxyethane)	17	17	0	-	-	[3]
Diiodomethane	50.8	50.8	0	0	0	[2]
Diiodomethane	50.8	49	1.8	0.01	0	[4]*
Diiodomethane	50.8	44.1	6.7	0.01	0	[4]**
Diiodomethane	50.8	48.5	2.3	0.01		[5]
Dimethylsulfoxide	44	36	8	0.5	32	[2]
Dodecane	25.35	25.35	0	0	0	"
Eicosane	28.87	28.87	0	0	0	"
Ethanol	22.4	18.8	2.6	0.019	68	"
Ethyl acetate (ethyl ethanoate)	23.9	23.9	0	0	6.2	[3]
Ethylene Glycol	48	29	19	1.92	47	[2]
Ethylene Glycol	48	29	19	3	30.1	[3]
Ethylene Glycol	48.8	32.8	16	3	30.1	[6]
Formamide	58	39	19	0.5	32	[2]
Formamide	58	39	19	2.28	39.6	[3]
Formamide	58.2	36	22.2	2.29	39.6	[4]*
Formamide	57.9	34.3	23.5	2.28	39.6	[6]
Formamide	58.2	39.5	18.7	2.28	39.6	[5]
Glycerol	64	34	30	3.92	57.4	[2]
Glycerol	63.4	40.6	22.8	3.92	57.4	[4]*
Glycerol	63.4	37	26.4	3.92	57.4	[6]
Heptane	20.14	20.14	0	0	0	[2]
Hexadecane	27.47	27.47	0	0	0	"
Hexane	18.4	18.4	0	0	0	"
Methanol	22.5	18.2	4.3	0.06	77	"
Methyl-ethyl-ketone	24.6	24.6	0	0	24	"
Nitrobenzene	43.9	41.3	2.6	0.26	6.6	"
Nonadecane	28.59	28.59	0	0	0	"
Nonane	22.85	22.85	0	0	0	"
Octane	21.62	21.62	0	0	0	"
Perfluoroheptane	12.8	12.8	0	0	0	[7]

Fluid/Solid	γ (mN/m)	γ^{LW} (mN/m)	γ^{AB} (mN/m)	γ^{+} (mN/m)	γ^{-} (mN/m)	Ref.
Perfluorohexane (FC-72)	12.0	(12.0)	(0)	(0)	(0)	[8]
Perfluorohexane (FC-72)	10.0	(10.0)	(0)	(0)	(0)	[9]
Pentadecane	27.07	27.07	0	0	0	[2]
Pentane	16.05	16.05	0	0	0	"
Silicone Oil	18.8	18.8	0	0	0	[10]
Tetradecane	26.56	26.56	0	0	0	[2]
Tetrahydrofuran	27.4	27.4	0	0	15	"
Tricresyl phosphate	40.9	39.8	1.1			[4]*
Tricresyl phosphate	40.9	39.7	1.2			[4]***
Tricresyl phosphate	40.9	39.2	1.7			[5]
Tridecane	25.99	25.99	0	0	0	[2]
Toluene	28.5	28.5	0	0	0.72	[3]
Undecane	24.66	24.66	0	0	0	[2]
Water	72.8	21.8	51	25.5	25.5	"
Water	72.8	22.6	50.2	25.5	25.5	[4]*
Water	72.8	22.1	50.7	25.5	25.5	[4]**
o-Xylene	30.1	30.1	0	0	0.58	[3]
α-Bromonaphthalene	44.4	44.4	0	0	0	[2]
2-Ethoxyethanol	28.6	23.6	5			[3]
Polyethylene oxide, PEO 6000	43	43	0	0	64	[1]
Dextran 10000	61.2	47.4	13.8	1	47.4	"
Fluorocarbon polymer, FC 721	9.41	9.15	0.24	0.16	0.76	[11]
Polydimethylsiloxane, PDMS	23.1	22.9	0.12	0	3.05	[12]
Poly(methyl methacrylate), PMMA	39-43	39-43	0	0	9.5-22.4	[13]
Poly(methyl methacrylate), PMMA	48.9	46.5	2.4	0.08	18.1	[14]
Poly(methyl methacrylate), PMMA	46.4	44.4	1.92	0.03	27.9	[12]
Polyvinyl acetate, PVAc	44.5	42.6	1.9	0.041	22.3	[14]
Polyvinyl chloride, PVC	43.7	43	0.7	0.04	3.5	[13]
Polyvinyl chloride, PVC	43.1	40.2	2.9	0.42	5.1	[14]
Polystyrene, PS	42	42	0	0	1.1	[13]
PS (based on advancing CA)	44.9	44.9	0	0	1.33	[15]
PS (based on receding CA)	49.9	49.9	0	0	5.14	"
Polyethylene, PE (based on advancing CA)	33	33	0	0	0.1	[13]
PE (based on receding CA)	57.9-62.5	42	15.9-20.5	2.1	30-50	"
Polyethylene glycol, PEG-silane-modified	47.9	45.3	2.59	0.04	39.92	[12]
Polyamide-imide, PAI	52.6	42.8	9.8	1.04	23.15	[16]
Polyhydroxyethylmethacrylate, PHEMA	50.6	40.2	10.4	2.07	13.1	[17]

Fluid/Solid	γ (mN/m)	γ^{LW} (mN/m)	γ^{AB} (mN/m)	γ^{+} (mN/m)	γ^{-} (mN/m)	Ref.
P(HEMA80/EMA20)	48.2	40.7	7.5	0.63	22.7	"
P(HEMA40/EMA60)	39.8	39.4	0.4	0.02	16.4	"
Polypyrrole, PPyTS	47	41	6	0.81	10.9	[18]
PPyCl	43.5	36.6	6.9	0.43	28.3	"
PPyDS	41.7	34.8	6.9	1.35	8.85	"
Poly(3-octylthiophene) (POT), undoped		22.5			0.5	[19]
POT-AuCl-4		23.4-25			0.7-4.7	"
Polystyrene, PS	41.9	41.9	0.22	0.08	0.15	[12]
PS latices (Anionic) (advancing)	41.4	41.4	0	0	13.13	[15]
PS latices (Anionic) (receding)	57.6	50.8	6.8	1.19	9.73	"
PS latices (Cationic) (using water/ethylene glycol)		39.4-41.9		0-0.4	0.3-7	"
PS latices (Cationic) (using water/formamide)		39.4-41.9		0-0.1	1.8-8.2	"
Polypropylene, PP	32.2	30.1	2.1	0.3	3.8	[20]
PP	25.7	25.7	0	0	0	[21]
PP	29.7	29.7	0	0	1.4	[22]
PP-O2 plasma	43.1	36.7	6.4	0.5	22	[20]
PP-N2 plasma	53.3	41.9	11.4	1	30.9	"
PP-NH3 plasma	42.6	34.9	7.7	0.7	21.4	"
Fluorinated ethylene-propylene (FEP)	15.71	15.42	0.34	0.01	0.72	[11]
FEP	18.3	18.3	0	0	0	[23]
Poly(tetrafluoroethylene), PTFE	19.6	19.6	0	0	0	[24, 25]
Poly(tetrafluoroethylene), PTFE	20.8	19.9	0.9	0.1	1.6	[3]
Polyisobutylene, PIS	25	25	0	0	0	[21, 25]
Polyaurinlactam, PA 12	41.9	37.5	4.4	1	4.9	[23]
Nylon (PA) 66	42.8	38.6	4.2	0.4	11.3	"
Nylon 66	37.7	36.4	1.3	0.02	21.6	[24, 26]
Polyvinyl pyrrolidone, PVPY	43.4	43.4	0	0	29.9	[25]
Polyvinyl fluoride, PVF	43.6	40.4	3.2	0.16	12.9	[27]
Polypropylene/EPDM, flame treated	43.7	25.9	17.8	2.6	30.3	[22]
Polyoxytretramethylene glycol), MW 2000	44	41.4	2.6	0.06	27.6	[28]
Polyoxyethylene, POE, PEG-6000	43	43	0	0	64	[29]
Polyethylene terephthalate	43.84	43.48	0.36	0.003	7.17	[11]
Ethylene glycol-*co*-propylene glycol, MW 2000	47.5	42	5.5	0.13	58.8	[28]
Ethylene glycol-*co*-propylene glycol, MW 1000	47.9	40.9	7	0.22	55.6	"

Fluid/Solid	γ (mN/m)	γ^{LW} (mN/m)	γ^{AB} (mN/m)	γ^{+} (mN/m)	γ^{-} (mN/m)	Ref.
Oriented polypropylene, OPP (advancing)	32.6	32.6	0	0	0	[30]
OPP (receding)	39.2	37	2.2	1.3	0.9	"
OPP-air Corona-treated (advancing)	55.8	42	13.9	1.9	25.2	"
OPP-air Corona-treated (receding)	64.7	46.2	18.5	2	25.2	"
Trimethoxy(octadecyl)silane (OTS)	23.5	23.3	0.19	0.01	1.1	[12]
Zoltek carbon fibers, unsized	41.3	41.3	0	0	32.4	[19]
Zoltek carbon fibers, Ultem sized	40.2	38.6	1.6	0.03	20.5	"
Zoltek carbon fibers, PU sized	35.8	33.2	2.6	0.11	15.3	"
Chromium	59.6	45.8	13.8	0.86	55.5	[14]
Aluminum	57.4	46.7	10.7	0.5	57.5	"
Silicon wafer	61.9	38.6	23.3	4	33.98	[31]
Glass	59.3	42.03	17.8	1.97	40.22	"
Glass, H2SO4/HNO3	64.5	42.03	22.47	2.82	44.76	"
Glass, C18	26.8	25.7	1.12	0.24	1.32	"
Glass, APS-treated	45	39.2	5.76	0.084	98.62	[12]
HSA, dry, pH 4.8	45	44	0.1	0.03	76	[32]
HSA, dry, pH 7	41.4	41	0.4	0.002	20	"
HSA, hydrated, pH 7	62.5	26.8	35.7	6.3	50.6	"
HIg-G, hydrated, pH 7	51.3	34	17.3	1.5	49.6	"
HIg-A, hydrated, pH 7	26.8	26.8	0	0	93	"
Bovine fibrinogen, dry	40.3	40.3	0	0	53.2	"
Human fibrinogen, dry	40.6	40.6	0	0	54.9	"
HLDLP, dry	41.1	35.5	5.66	0.26	30.8	"
Candida abicans (yeast) cultured at 30C	42.5	38.1	4.4	2.9	1.7	[33]
Candida abicans (yeast) cultured at 37C	47.7	37.3	10.4	0.6	43.7	"
Streptococcus gordonii (bacteria) cultured at 37C	38.9	35.8	3.1	4.2	0.6	"
Streptococcus oralis 34	57	35	22	2.7	45	[34]
Streptococcus oralis J22	48.7	38	10.68	0.5	57	"
Actinomyces naeslundii 5951	44	38	6	0.5	18	"
Actinomyces naeslundii 5519	40	37	2.97	0.1	22	"
Pressure-sensitive adhesive, PSA	16.7	12.6	4.1	0.42	9.9	[14]
Cellulose acetate	40.2	35	5.2	0.3	22.7	[13]
Cellulose nitrate	45	45	0	0	16	[13]
Agarose	44.1	41	3.1	0.1	24	"
Gelatin	38	38	0	0	19	"

Fluid/Solid	γ (mN/m)	γ^{LW} (mN/m)	γ^{AB} (mN/m)	γ^{+} (mN/m)	γ^{-} (mN/m)	Ref.
Paraffin	25.5	25.5	0	0	0	[35]
Krytox 100	15.9	11.7	0.115	0.016	0.200	[36]
Krytox 105	18.8	12.7	0.049	0.028	0.021	"
Trichloro(1H,1H,2H,2H-perfluorooctyl)silane (TFTS) (advancing contact angles)	8.0	7.6	0.48	0.64	0.09	[37]
Trichloro(1H,1H,2H,2H-perfluorooctyl)silane (TFTS) (receding contact angles)	24.5	24.9	0.48	0.01	5.76	"
Trichloro(1H,1H,2H,2H-perfluorooctyl)silane (TFTS) (23 °C anneal)	17.07	11.28	3.38	2.36	1.21	[38]
Trichloro(1H,1H,2H,2H-perfluorooctyl)silane (TFTS) (150 °C anneal)	8.41	5.35	2.47	2.68	0.57	"
Trichloro(3,3,3-trifluoropropyl) silane (FPTS) (23 °C anneal)	29.05	18.01	4.70	3.43	1.61	"
Trichloro(3,3,3-trifluoropropyl) silane (FPTS) (150 °C anneal)	14.48	10.62	0.40	3.72	0.11	"
Clean glass (advancing contact angles)	51.1	40.8	10.92	0.49	60.84	[37]

*from contact angle measurement

**from interfacial tension measurement

***from contact angle data on poly(methyl methacrylate)

(parenthesis) indicate estimated value

S2. Determination of vOCG Surface Energy Components

The vOCG surface energy components for undocumented fluids were determined by plane fitting experimental data points determined from at least three different test fluids. In the present work, the test fluids water, glycerol, ethylene glycol, 1-bromonapthalene, and chloroform were chosen. Equation S1 shows the form of the plane equation, where the left-hand-side corresponds to the vertical axis in Figure S1 and the right hand side contains two slope terms and the intercept. The subscript "u" indicates the fluid with unknown vOCG components which must be solved for, the subscript "i" represents the i-th test fluid for which the vOCG terms are known, and the interfacial tensions γ_u and γ_{ui} are measured experimentally.

$$\frac{(\gamma_u + \gamma_i) - \gamma_{ui}}{\sqrt{\gamma_i^{LW}}} = \sqrt{\gamma_u^+}\sqrt{\frac{\gamma_i^-}{\gamma_i^{LW}}} + \sqrt{\gamma_u^-}\sqrt{\frac{\gamma_i^+}{\gamma_i^{LW}}} + 2\sqrt{\gamma_u^{LW}} \tag{S1}$$

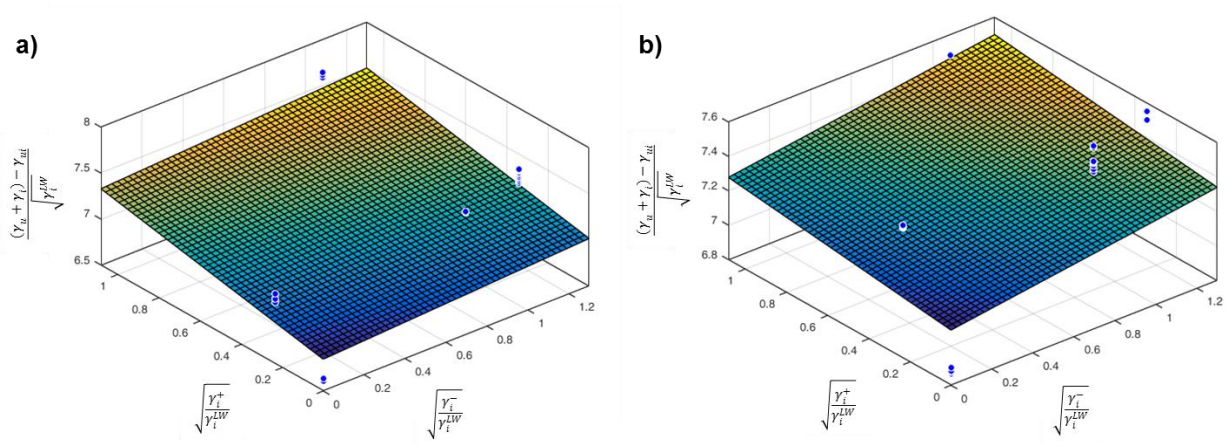

Figure S1. Planar regression to determine vOCG surface energy components. Each measurement in the pendant drop experiment is represented by a point on the plot. The intercept and two slopes give the best-fit values for the LW, acid, and base surface energy components. The regression is shown here for (a) Krytox GPL 100 and (b) Krytox GPL 105 with results shown in Table S1 above, and the error from this process was determined to be less than 1 mN/m for each of the predicted surface energy components. A linear interpolation/extrapolation with these values may be used to approximate the surface energy components of Krytox GPL oils ranging from 100-107.

S3. Impact of Surface Geometry

The surface geometric factor R is determined by the roughness, r, which represents the actual solid surface area divided by the projected area, and the solid fraction, φ, which represents the fraction of the solid which contacts the base of the droplet. These properties are combined in the form $R = (r–1)/(r–\varphi)$, where R can vary from 0 for a flat surface to 1 for an extremely rough surface, shown in Figure S2. A higher value of R amplifies the interaction between the solid and either of the liquid phases compared to the liquid phases with each other or with the surrounding vapor. For instance, increasing R can satisfy criterion (III) for a given lubricant which does not spontaneously spread over a flat solid surface.

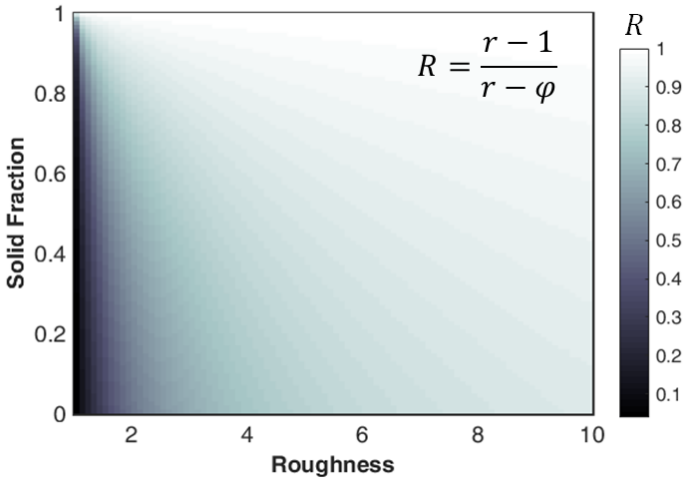

Figure S2. Plot of the geometric factor *R*. Values for R range from 0, corresponding to a flat surface, to 1, corresponding to a very rough surface.

S4. Effect of Tightening the Miscibility Constraint

The miscibility criterion (V) in the main text can be more generally written as:

$$\gamma_{dl} > \gamma_m \tag{S2}$$

where γ_m is a miscibility cutoff value. All predictions in the main text use a cutoff value of γ_m = 0 mN/m unless otherwise indicated. The effect of altering the miscibility cutoff is explored here, with the result displayed in Figure S3.

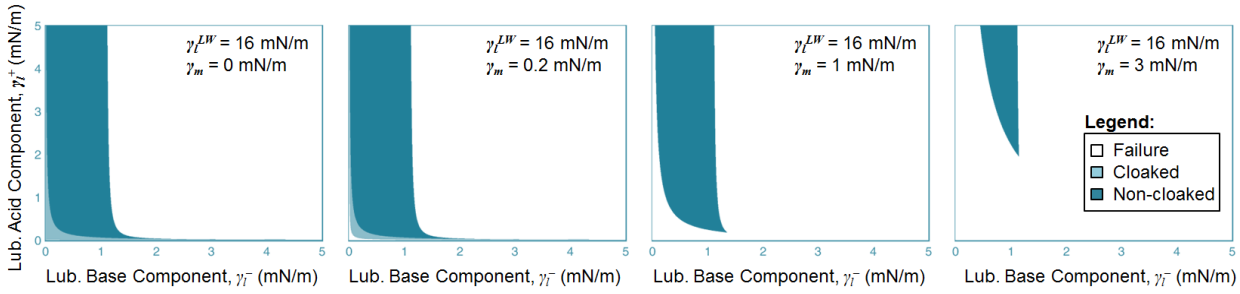

Figure S3. Result of changing the miscibility cutoff, γ_m. A higher miscibility cutoff results in a more conservative solution (i.e., more stringent requirement to be considered immiscible) which makes the solution domain smaller. Conversely, setting γ_m to $-\infty$ is equivalent to removing criterion (V) from the model.

The optimal miscibility cutoff was calculated from a dataset comprised of 120 fluid-fluid interactions with known miscibility (binary values: either miscible or immiscible).[39] Only 20% of the cases in the dataset were for two immiscible fluids, with the remainder of the cases representing two miscible fluids. With this in mind, a successful prediction for two immiscible fluids was scored 4x higher than a successful prediction for two miscible fluids to avoid a bias in prediction capability towards miscible pairs, resulting in a maximum attainable score of 192 for the 120 cases corresponding to 100% prediction accuracy. The vOCG-based miscibility prediction (Equation 7 from the main text) was performed for all of the fluid pairs in the dataset, and the score based on the number of correct predictions was determined.

The prediction score was bounded by 50% accuracy at a cutoff of $-\infty$ when every prediction is immiscible (i.e., 50% agreement between the vOCG prediction and the dataset representing only the immiscible cases, 20% of the 120 cases scored with 4x weight for a total of 96 out of 192 points) and 50% accuracy at a cutoff of $+\infty$ when every prediction is miscible (i.e., 50% agreement between the vOCG prediction and the dataset representing only the immiscible cases, 80% of the 120 cases scored with 1x weight for a total of 96 out of 192 points). The scores between these bounds are plotted in Figure S4. The optimal cutoff for miscibility was found to be 3.5 mN/m based on this scoring algorithm, as it resulted in the highest likelihood of predicting either miscibility or immiscibility correctly. This cutoff will give a more conservative prediction

of whether a proposed LIS will succeed or fail if used in criterion (V). In the main text, the miscibility cutoff value of γ_m = 0 mN/m was used throughout to avoid the requirement for empirical data, but this more conservative "fitting parameter" miscibility cutoff value of γ_m = 3.5 mN/m could be used to help eliminate spurious results in future work.

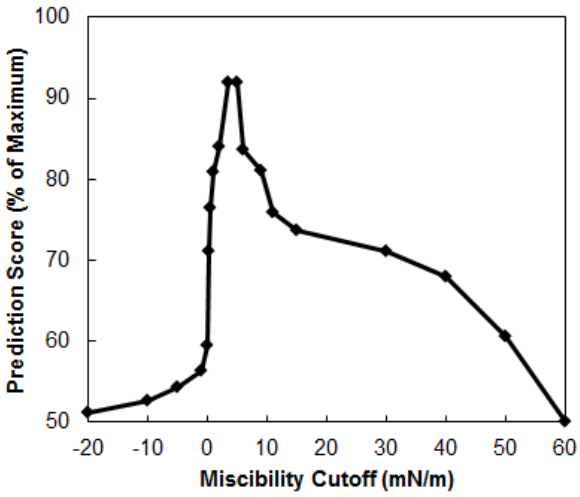

Figure S4. Weighted miscibility prediction score versus miscibility cutoff value. The optimal value for accurate miscibility prediction is 3.5 mN/m, which could be used in criterion (V) instead of 0 mN/m for a more conservative prediction of whether a LIS surface will succeed.

S5. Choice of Solid Material for Polar Impinging Fluids

Figure 2 in the main text demonstrated the suitability of polar surfaces with significant Lewis acid-base components of vOCG surface energy for repulsion of nonpolar impinging fluids. However, if the impinging fluid is very polar, a nonpolar solid surface will likely generate a larger solution domain as shown in Figure S5 with water as the impinging fluid.

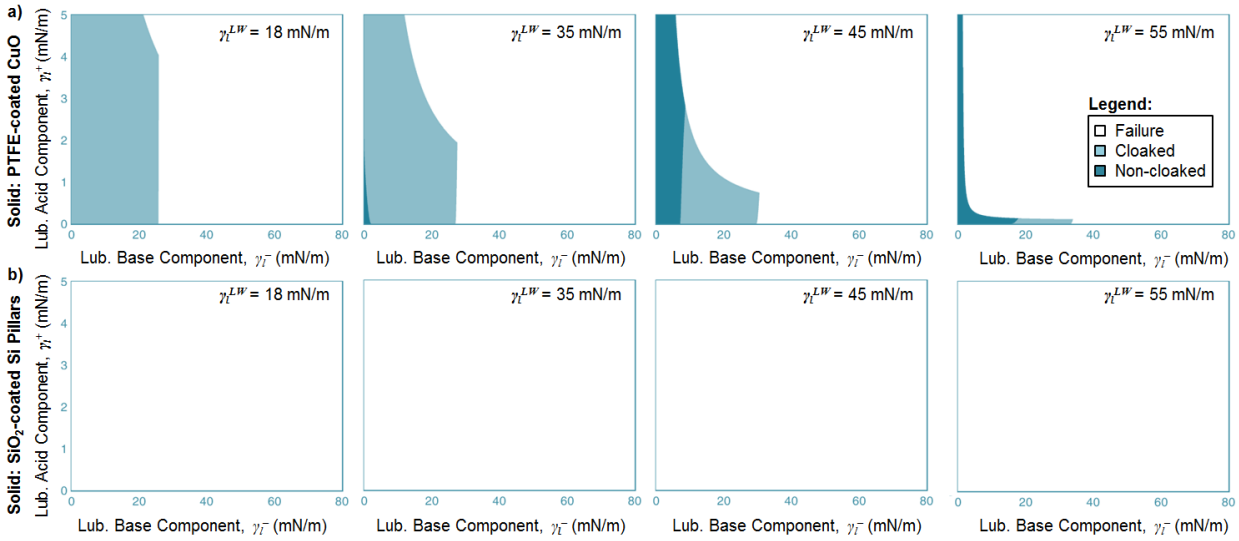

Figure S5. Design of LIS to repel a polar fluid – in this case, water. The PTFE-coated solid surface allows a reasonable solution domain of fluid choices, shown in (a). The polar SiO_2 pillar array surface does not result in any solutions for practical lubricating fluids (solutions only exist for $\gamma^+ > 20$ mN/m, which is outside of the realm of available choices as illustrated in Table S1), shown in (b).

S6. Results from Condensation Experiments

Images of several successful condensation tests performed with various fluids on a LIS are shown in Figure S6. These results were used in Table 1 for the model validation.

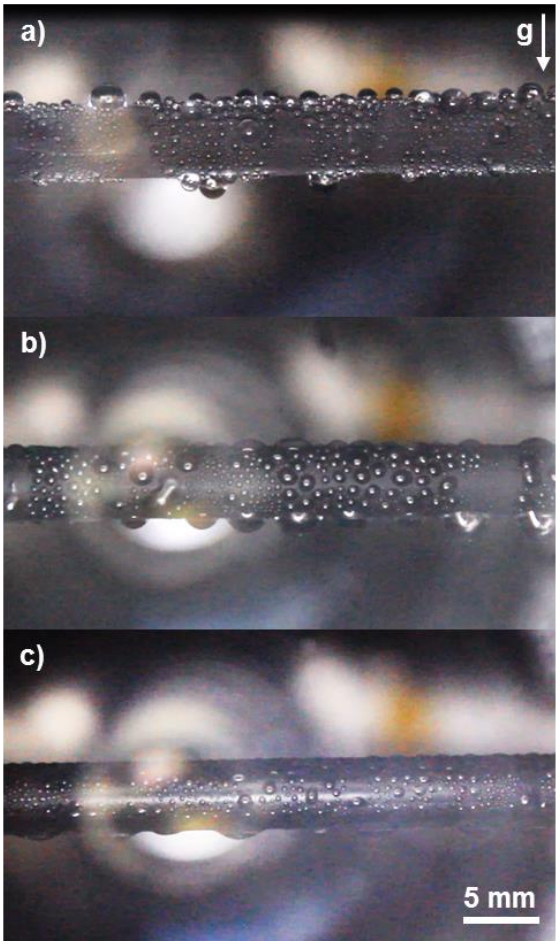

Figure S6. Results from condensation of impinging fluids on LIS. Three different impinging fluids, (a) water, (b) toluene, and (c) pentane, were condensed onto a LIS comprised of Krytox GPL 101 infused into TFTS-coated CuO nanoblades. In all three cases, formation of discrete droplets of condensate was observed.

S7. Droplet Impingement Experimental Setup

Experiments were performed for the LIS using SiO_2-coated pillar arrays fabricated on silicon wafers as the solid. The geometric factor of the pillar array used was $R = 0.71$. Since these high-surface-energy SiO_2-coated pillars could not be applied to the exterior of the cylindrical condenser tubes, droplet impingement tests were performed to determine whether the proposed LIS designs were successful. The experimental setup is shown schematically in Figure S7.

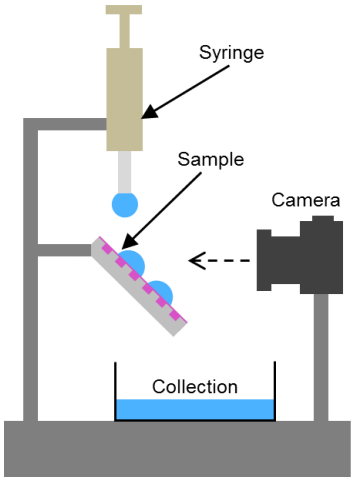

Figure S7. Droplet impingement experimental setup. The droplets were dispensed from a syringe onto the sample, which was mounted at an angle beneath the syringe and in front of the camera. Departing impinging droplets fell into a collection vessel. The entire experimental setup was contained within a fume hood.

S8. Reduction in Landau-Notation Order of Required Experiments

In terms of characterization of LIS from empirical measurements, certainly the direct measurement of interfacial energies, contact angles, spreading parameters, or other equivalent data to individually characterize each unique interface in a particular LIS system is reasonable for a relatively small set of phases, as has been performed in past work to describe experimentally observed LIS behaviour for sets of 1-2 solids, 1-3 lubricants, and <10 impinging fluids. However, as the number of possible solid, lubricant, and impinging fluid phases becomes large (as when exploring the full range of possible materials), direct interfacial characterization becomes intractable. Considering N total phases divided equally between solids, lubricants, and impinging fluids, the total number of surface energy components required to use the vOCG method to characterize every combination of fluids scales as $O(N)$. Meanwhile, the number of unique interfaces formed between phases that would require experimental characterization scales as $O(N^3)$. To determine the behavior of each unique LIS combination for only 30 of each phase (30 solids, 30 lubricants, and 30 impinging fluids) would require 270 experimentally measured

vOCG surface energy components for complete characterization with the model proposed in the present work. Conversely, if each unique interface were experimentally characterized as in past work, 27,000 experiments would need to be conducted, presumably requiring 100x more effort. Additionally, many commonly available phases have already had their vOCG surface energy components characterized; a table with vOCG surface energy components for over 150 phases is included in the Supporting Information section S1 above.

S9. Effect of Gravity on Lubricant Drainage

Gravity has the potential to partially deplete the lubricant from a LIS if the capillary pressure is not sufficient to hold the lubricant within the surface structures. For a tilted surface, illustrated schematically in Figure S8, the capillary pressure can support the gravitational body force acting on the lubricant up to a maximum value, $P_{cap,max}$ based on the lubricant and surface chemistries and the surface structure geometry.

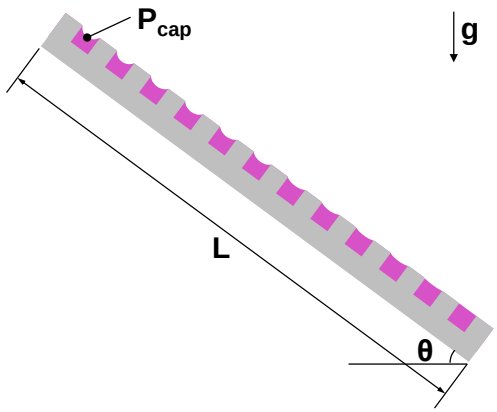

Figure S8. Schematic illustrating contribution of gravity to LIS failure. The gravitational body force on the lubricant is counteracted by the Laplace pressure due to the curvature of the lubricant interface. If the maximum capillary pressure is not sufficient to support the gravitational body force, the lubricant will not cover the entire surface.

The maximum capillary pressure can be estimated from a commonly used method that considers the change in total surface energy as a given fluid volume propagates through a structured surface[40]:

$$P_{cap,max} = \frac{-\Delta E}{\Delta V} \tag{S3}$$

where $-\Delta E$ is the change in surface energy and ΔV is the change in volume. For a structured surface comprised of a square array of pillars, Equation S3 simplifies to:

$$P_{cap,max} = \frac{\gamma_s - (\gamma_{ls} + \gamma_l) + \gamma_l R}{H(1-\varphi)} \tag{S4}$$

where the numerator is simply the left-hand-side of Equation 10, for criterion (III), in the main text. Once the maximum capillary pressure is determined with Equation S4, the maximum surface length, L_{max}, that will remain stable in the presence of gravity is:

$$L_{max} = \frac{P_{cap,max}}{\rho g \sin(\theta)} \tag{S5}$$

For example, taking the SiO_2 pillar array in the main text, with $R = 0.71$ and $\varphi = 0.096$, tilted at approximately 45° and with methanol as the lubricant, we find that the surface length at which gravitational lubricant depletion occurs is over 500 m, which is much larger than the sample length of 0.02 m used in the experiments in this work. Even the surface length required for gravitational lubricant depletion with diiodomethane (which has a lower attraction to SiO_2 and a higher density than methanol) as the lubricant is over 50 m, indicating that gravitational lubricant depletion did not play a role in the experiments in the present work.

Supporting Information References

1 van Oss, C. J. & Good, R. J. Prediction of the Solubility of Polar Polymers by Means of Interfacial-Tension Combining Rules. *Langmuir* **8**, (1992).

2 Etzler, F. M. Determination of the Surface Free Energy of Solids. *Rev. Adhesion Adhesives* **1**, (2013).

3 *Surface Tension Components and Molecular Weight of Selected Liquids*, <https://www.accudynetest.com/surface_tension_table.html> (2017).

4 Wu, S. *Polymer interface and adhesion*. (M. Dekker, 1982).

5 Carre, A. Polar interactions at liquid/polymer interfaces. *Journal of Adhesion Science and Technology* **21**, (2007).

6 Mittal, K. L. *Contact angle, wettability and adhesion*. (VSP, 2009).

7 Binks, B. P. & Clint, J. H. Solid wettability from surface energy components: Relevance to pickering emulsions. *Langmuir* **18**, (2002).

8 Rykaczewski, K., Paxson, A. T., Staymates, M., Walker, M. L., Sun, X. D., Anand, S., Srinivasan, S., McKinley, G. H., Chinn, J., Scott, J. H. J. & Varanasi, K. K. Dropwise condensation of low surface tension fluids on omniphobic surfaces. *Scientific Reports* **4**, (2014).

9 Liu, T. Y. & Kim, C. J. Turning a surface superrepellent even to completely wetting liquids. *Science* **346**, (2014).

10 Chan, D., Hozbor, M. A., Bayramli, E. & Powell, R. L. Surface Characterization of Intermediate Modulus Graphite Fibers Via Surface Free-Energy Measurement and Esca. *Carbon* **29**, (1991).

11 Kwok, D. Y., Li, D. & Neumann, A. W. Evaluation of the Lifshitz Van-Der-Waals Acid-Base Approach to Determine Interfacial-Tensions. *Langmuir* **10**, (1994).
12 Wang, H. & Newby, B. M. Z. Applicability of the extended Derjaguin-Landau-Verwey-Overbeek theory on the adsorption of bovine serum albumin on solid surfaces. *Biointerphases* **9**, (2014).
13 Lee, L.-H. *Fundamentals of adhesion*. (Plenum Press, 1991).
14 McCafferty, E. & Wightman, J. P. Determination of the acid base properties of metal oxide films and of polymers by contact angle measurements. *Apparent and Microscopic Contact Angles*, (2000).
15 Bouali, B., Ganachaud, F., Chapel, J. P., Pichot, C. & Lanteri, P. Acid-base approach to latex particles containing specific groups based on wettability measurements. *Journal of Colloid and Interface Science* **208**, (1998).
16 van Oss, C. J., Giese, R. F. & Good, R. J. Reevaluation of the Surface-Tension Components and Parameters of Polyacetylene from Contact Angles of Liquids. *Langmuir* **6**, (1990).
17 Good, R. J., Islam, M., Baier, R. E. & Meyer, A. E. The effect of surface hydrogen bonding (acid-base interaction) on the hydrophobicity and hydrophilicity of copolymers: Variation of contact angles and cell adhesion and growth with composition. *Journal of Dispersion Science and Technology* **19**, (1998).
18 Azioune, A., Chehimi, M. M., Miksa, B., Basinska, T. & Slomkowski, S. Hydrophobic protein-polypyrrole interactions: The role of van der Waals and Lewis acid-base forces as determined by contact angle measurements. *Langmuir* **18**, (2002).
19 Fadda, E. & Clarisse, C. Characterization of the Surface Modifications of Conducting Poly(3-Octylthiophene) Films by Contact-Angle Measurements. *Synthetic Metals* **72**, (1995).
20 Bodino, F. Ph.D. thesis, Faculte´s Universitaires Notre-Dame de la Paix, (1998).
21 van Oss, C. J., Chaudhury, M. K. & Good, R. J. The Mechanism of Phase-Separation of Polymers in Organic Media - Apolar and Polar Systems. *Separation Science and Technology* **24**, (1989).
22 Jacobasch, H. J., Grundke, K., Schneider, S. & Simon, F. Surface Characterization of Polymers by Physico-Chemical Measurements. *The Journal of Adhesion* **48**, (1995).
23 Chibowski, E. & Gonzalezcaballero, F. Interpretation of Contact-Angle Hysteresis. *Journal of Adhesion Science and Technology* **7**, (1993).
24 van Oss, C. J., Good, R. J. & Busscher, H. J. Estimation of the Polar Surface-Tension Parameters of Glycerol and Formamide, for Use in Contact-Angle Measurements on Polar Solids. *Journal of Dispersion Science and Technology* **11**, (1990).
25 van Oss, C. J. & Good, R. J. Surface Tension and the Solubility of Polymers and Biopolymers: The Role of Polar and Apolar Interfacial Free Energies. *Journal of Macromolecular Science: Part A - Chemistry* **26**, (1989).
26 Janczuk, B., Chibowski, E., Bruque, J. M., Kerkeb, M. L. & Caballero, F. G. On the Consistency of Surface Free-Energy Components as Calculated from Contact Angles of Different Liquids - an Application to the Cholesterol Surface. *Journal of Colloid and Interface Science* **159**, (1993).
27 Hollander, A. On the Selection of Test Liquids for the Evaluation of Acid-Base Properties of Solid-Surfaces by Contact-Angle Goniometry. *Journal of Colloid and Interface Science* **169**, (1995).

28 van Oss, C. J. *Interfacial forces in aqueous media*. (M. Dekker, 1994).
29 van Oss, C. J., Chaudhury, M. K. & Good, R. J. Monopolar Surfaces. *Advances in Colloid and Interface Science* **28**, (1987).
30 Good, R. J., Shu, L. K., Chiu, H. C. & Yeung, C. K. Hydrogen bonding and the interfacial component of adhesion: Acid/base interactions of corona-treated polypropylene. *Journal of Adhesion* **59**, (1996).
31 Freitas, A. M. & Sharma, M. M. Effect of surface hydrophobicity on the hydrodynamic detachment of particles from surfaces. *Langmuir* **15**, (1999).
32 van Oss, C. J. *Forces Interfaciales En Milieux Aqueux*. (1996).
33 Millsap, K. W., Bos, R., Busscher, H. J. & van der Mei, H. C. Surface Aggregation of Candida albicanson Glass in the Absence and Presence of Adhering Streptococcus gordonii in a Parallel-Plate Flow Chamber: A Surface Thermodynamical Analysis Based on Acid–Base Interactions. *Journal of Colloid and Interface Science* **212**, (1999).
34 Bos, R. & Busscher, H. J. Role of acid-base interactions on the adhesion of oral streptococci and actinomyces to hexadecane and chloroform - influence of divalent cations and comparison between free energies of partitioning and free energies obtained by extended DLVO analysis. *Colloids and Surfaces B-Biointerfaces* **14**, (1999).
35 Janczuk, B., Bialopiotrowicz, T. & Zdziennicka, A. Some remarks on the components of the liquid surface free energy. *Journal of Colloid and Interface Science* **211**, (1999).
36 Present Work.
37 Smith, J. D. *Hydrate-phobic surfaces*, Massachusetts Institute of Technology, (2011).
38 Chen, J. K., Ko, F. H., Hsieh, K. F., Chou, C. T. & Chang, F. C. Effect of fluoroalkyl substituents on the reactions of alkylchlorosilanes with mold surfaces for nanoimprint lithography. *Journal of Vacuum Science & Technology B* **22**, (2004).
39 Phenomenex_Publications. A User's Guide to Gel Permeation Chromatography. (2000).
40 Xiao, R., Enright, R. & Wang, E. N. Prediction and Optimization of Liquid Propagation in Micropillar Arrays. *Langmuir* **26**, (2010).